

1 **PACT suppresses PKR activation through dsRNA binding and dimerization, and is a**
2 **therapeutic target for triple-negative breast cancer**

3 Addison A. Young ¹, Isabelle G. Juhler ¹, Jackson R. Pierce ¹, Holly E. Bohlin ¹, Haley A. Harper
4 ², David S. Onishile ¹, Renee N. Chua ¹, Madison E. Liu ¹, Estelle N. Gardner ¹, Bennett D. Elzey
5 ^{2,3}, Kyle A. Cottrell ^{1,2}

6 ¹Department of Biochemistry, Purdue University, West Lafayette, IN, USA

7 ²Purdue Institute for Cancer Research, Purdue University, West Lafayette, IN, USA

8 ³Department of Comparative Pathobiology, Purdue University, West Lafayette, IN, USA

9 The authors declare no potential conflicts of interest.

10

11 Correspondence:

12 Kyle A Cottrell, Ph.D.
13 Department of Biochemistry
14 Purdue University
15 201 S University St.
16 West Lafayette, IN
17 Email: kacottre@pudue.edu
18 Telephone: 765-494-6941
19

20 Shortened title: PACT suppresses PKR activation in TNBC

21

22 Keywords: dsRNA, cancer, PACT, ADAR1, RBP, PKR

23

24

25 **Abstract**

26 Triple-negative breast cancer (TNBC), the deadliest breast cancer subtype, lacks broadly
27 applicable targeted therapies. Induction of 'viral mimicry' by activation of viral double-stranded
28 RNA (dsRNA) sensors has potential therapeutic applications for TNBC and other cancers.
29 Suppressors of dsRNA sensing prevent sensing of endogenous dsRNAs and resulting
30 autoimmunity. Depletion of the suppressor of dsRNA sensing ADAR1 causes activation of
31 dsRNA sensors and cell death in many cancer cell lines. These ADAR1-dependent cells are
32 generally also dependent on the dsRNA-binding protein PACT, which is highly expressed and
33 essential in many TNBC cell lines. While PACT is known as an activator of the dsRNA sensor
34 PKR, overexpression of PACT had no effect on activation of PKR in multiple TNBC cell lines.
35 Conversely, depletion of PACT in PACT-dependent cell lines caused robust activation of the
36 dsRNA sensor PKR and cell death, in addition to induction of integrated stress response genes
37 and NF- κ B targets. These phenotypes were entirely dependent on PKR. Rescue experiments
38 revealed that PACT dimerization and dsRNA binding is required to suppress PKR activation.
39 While depletion of PACT alone in ADAR1/ PACT-independent cell lines had no effect on PKR
40 activation, combined depletion of both PACT and ADAR1 in those cell lines caused robust PKR
41 activation and cell death, supporting a partially redundant role for ADAR1 and PACT in
42 suppression of dsRNA sensing. Taken together, these findings support a vital role for PACT in
43 suppressing PKR activation and highlight the therapeutic potential of targeting PACT to treat
44 TNBC.

45

46

47 **Introduction**

48 Triple-negative breast cancer (TNBC) is the deadliest form of breast cancer, with high
49 rates of recurrence and metastasis (Curigliano and Goldhirsch 2011; Bianchini et al. 2016). A
50 major factor driving the poor outcomes of TNBC patients is the lack of broadly applicable
51 targeted therapies for TNBC (Curigliano and Goldhirsch 2011; Bianchini et al. 2016; Waks and
52 Winer 2019). Immunotherapies, such as immune checkpoint blockade (ICB), have shown some
53 efficacy in TNBC, but many tumors are resistant (Morad et al. 2021). Often, tumors with
54 increased inflammation, known as immunologically 'hot' (immune inflamed), are more sensitive
55 to ICB, relative to 'cold' (immune excluded) tumors (Chen and Mellman 2017). Several recent
56 studies have shown that increasing inflammation within tumors can overcome resistance to ICB
57 (Ishizuka et al. 2019; Jiang et al. 2019; Guirguis et al. 2023; Huang et al. 2024; Young et al.
58 2024). A great example of this approach is targeting the RNA editor ADAR1 to overcome
59 resistance to ICB in mouse tumor models (Ishizuka et al. 2019).

60 Adenosine Deaminase Acting on RNA (*ADAR*, which encodes ADAR1) has been
61 identified as an essential gene in multiple cancer cell lines – including those derived from
62 breast, lung and ovarian cancer (Gannon et al. 2018; Liu et al. 2019; Kung et al. 2021). ADAR1
63 deaminates adenosine to inosine in double-stranded RNAs (dsRNA) in a process known as A-
64 to-I editing (Bass and Weintraub 1988; Bass 2024; Mendoza and Beal 2024). This function of
65 ADAR1 is essential and prevents autoimmunity. Specifically, A-to-I editing by ADAR1 prevents
66 activation of MDA5, a double-stranded RNA (dsRNA) sensor, by endogenous dsRNAs
67 (Liddicoat et al. 2015; Pestal et al. 2015). There are multiple dsRNA sensors expressed in
68 immune and non-immune cells that detect dsRNA arising from viral infections (Rehwinkel and
69 Gack 2020; Chen and Hur 2022; Cottrell et al. 2024a). Because these proteins bind to dsRNA
70 by recognizing the structure of the dsRNA, and generally lack any sequence specificity, dsRNA
71 sensors can also be activated by endogenous dsRNAs (Cottrell et al. 2024a). Several dsRNA
72 sensors, including MDA5 and RIG-I, activate the type-I interferon (IFN-I) pathway to promote an

73 antiviral response (Rehwinkel and Gack 2020). The dsRNA sensor protein kinase RNA-
74 activated (PKR) instead activates the integrated stress response (ISR) by phosphorylation of
75 eIF2 α and promotes inflammation through activation of NF- κ B (Gal-Ben-Ari et al. 2018;
76 Chukwurah et al. 2021).

77 Since dsRNA sensors can bind and be activated by endogenous dsRNAs, to prevent
78 autoimmunity, their activation must be suppressed in the absence of a viral infection. Multiple
79 proteins suppress activation of dsRNA sensors by endogenous dsRNAs. These ‘suppressors of
80 dsRNA sensing’, function through several mechanisms. For instance, ADAR1 prevents
81 activation of two different dsRNA sensors through distinct mechanisms. Whereas ADAR1
82 prevents activation of MDA5 through A-to-I editing of dsRNA, ADAR1 also prevents activation of
83 PKR through competition for dsRNA binding (Liddicoat et al. 2015; Pestal et al. 2015; Chung et
84 al. 2018; Hu et al. 2023). The activation of dsRNA sensors and their downstream pathways,
85 triggered by the loss of suppressors of dsRNA sensing or other perturbations, is referred to as
86 ‘viral mimicry’. This term reflects cell behavior similar to that elicited by viral infection, but
87 instead the cells are responding to endogenous dsRNAs (Chen et al. 2021; Cottrell et al.
88 2024a). It is this viral mimicry phenotype that overcomes resistance to ICB in ADAR1 depleted
89 tumors and serves as a strong justification for the identification of ADAR1 inhibitors to treat
90 multiple cancers (Ishizuka et al. 2019).

91 While the effects of depleting ADAR1 in cancer cells has therapeutic value, not all
92 cancer cells are dependent on ADAR1 for proliferation (Gannon et al. 2018; Liu et al. 2019;
93 Kung et al. 2021). We and others have observed that depletion of ADAR1 causes cell death
94 and/or reduced proliferation and activation of dsRNA sensors in only a subset of cancer cell
95 lines. Roughly half of TNBC lines are dependent on ADAR1 expression, based on reduced gene
96 dependency scores from DepMap (McFarland et al. 2018; Dempster et al. 2019; Broad 2024a).
97 In these ADAR1-dependent cell lines, depletion of ADAR1 causes cell death and activation of
98 multiple dsRNA sensing pathways (Gannon et al. 2018; Liu et al. 2019; Kung et al. 2021).

99 Conversely, in ADAR1-independent cell lines, depletion of ADAR1 has no effect on cell viability
100 and there is no activation of dsRNA sensors. One factor driving ADAR1-dependency is elevated
101 expression of IFN stimulated genes (ISGs) in ADAR1-dependent cell lines. The chronic IFN-I
102 signaling in these cells leads to elevated expression of dsRNA sensors (PKR, MDA5, OAS1-3)
103 that are ISGs (Gannon et al. 2018; Liu et al. 2019; Kung et al. 2021). It has been proposed that
104 the elevated expression of dsRNA sensors in these cells creates a poised state, where the cells
105 are highly sensitive to loss of ADAR1 – or potentially the loss of other suppressors of dsRNA
106 sensing.

107 ADAR1 is not the only suppressor of dsRNA sensing. For example, DHX9 and STAU1
108 prevent PKR activation through binding to dsRNAs (Elbarbary et al. 2013; Cottrell et al. 2024b).
109 Like ADAR1, those proteins bind dsRNA through dsRNA binding domains (dsRBD). There are
110 nineteen human proteins that contain dsRBDs, and many other dsRNA binding proteins
111 (dsRBP) that bind via other domains, in particular helicase domains. Each of these proteins are
112 potentially competing with PKR, or perhaps MDA5, for binding to endogenous dsRNAs.

113 Here we provide evidence that protein activator of the interferon-induced protein kinase
114 (PACT) functions as a suppressor of dsRNA sensing in TNBC. We show that PACT specifically
115 suppresses PKR activation through dimerization and dsRNA binding. In addition to PKR
116 activation and cell death, depletion of PACT causes activation of the ISR and NF- κ B pathways
117 in PACT-dependent cell lines. In PACT-independent cell lines, our data support redundancy
118 between PACT and ADAR1 in suppression of dsRNA sensing. Together, our findings support
119 PACT as a therapeutic target for a subset of TNBC.

120 **Results**

121 **PACT is highly expressed in TNBC and essential in many TNBC cell lines**

122 Since ADAR1-dependent cell lines have elevated expression of PKR and other dsRNA
123 sensors, we hypothesized that they would be sensitive to loss of other suppressors of dsRNA
124 sensing. As such, we turned to publicly available gene dependency data from DepMap to

125 identify dsRBPs that may function as suppressors of dsRNA sensing like ADAR1. We
126 determined the pairwise correlation coefficients for ADAR1-dependency scores vs the
127 dependency scores for all other genes across all cell lines for which dependency data is
128 available in DepMap (Broad 2024b). This analysis was performed for dependency scores from
129 CRISPR-Cas9 screens (CHRONOS) and RNAi screens (DEMETER2) (McFarland et al. 2018;
130 Dempster et al. 2019). Among the genes with the strongest correlation with ADAR1-dependency
131 scores was *PRKRA*, which encodes PACT, (Pearson $r = 0.341$ for CHRONOS and 0.420 for
132 DEMETER2), (Fig. 1a-b; Supplemental Fig. S1a-b). While there are many other genes with
133 dependency scores that significantly correlate with ADAR1-dependency, including the RNA
134 exonuclease *XRN1* which has previously been shown to suppress activation of dsRNA sensors
135 (Zou et al. 2024), we decided to focus our research on PACT because it, like ADAR1, contains
136 multiple dsRNA binding domains. Additionally, PACT was the only dsRBD containing protein
137 with gene dependency scores that strongly correlate ($r > 0.2$) with ADAR1-dependency
138 (Supplemental Fig. S1c).

139 Analysis of pairwise correlation between PACT-dependency scores and those of all
140 other genes revealed ADAR1 as the strongest co-dependent gene of PACT (Fig 1c;
141 Supplemental Fig. S1d). Looking across lineages, PACT-dependent cell lines are common in
142 cancers arising from multiple organs (Fig. 1d; Supplemental Fig. S1e). Given our past efforts
143 studying ADAR1 in breast cancer, the strong correlation between PACT-dependency and
144 ADAR1-dependency scores in breast cancer cell lines (Fig. 1e and Supplemental Fig. S1f), and
145 several breast cancer cell lines being among the most strongly dependent on PACT, we chose
146 to focus on studying the role of PACT in breast cancer. Analysis of PACT-dependency in breast
147 cancer subtypes revealed a strong bias towards triple-negative breast cancer (TNBC) (Fig. 1f;
148 Supplemental Fig. S1g-i). Interestingly, the difference between PACT-dependency scores
149 amongst TNBC versus non-TNBC cell lines is larger than the difference for all but two other
150 genes (Fig. 1g).

151 The expression of PACT at the RNA and protein levels varies across cell lines, with
152 TNBC cell lines generally expressing more PACT than non-TNBC lines (Fig. 2a, Supplemental
153 Fig. S2a-b). In human tumors, PACT expression is significantly elevated in TNBC relative to
154 normal breast or other subtypes, (Fig. 2d-e and Supplemental Fig. S2c-d). Elevated expression
155 of PACT, however, is not prognostic of survival in breast cancer overall, or TNBC (Fig. 2f-g).

156 **PACT is not an activator of PKR in TNBC**

157 Previous research has indicated that PACT is an activator of the dsRNA sensor PKR
158 (Patel and Sen 1998; Patel et al. 2000; Peters et al. 2001; Li et al. 2006; Peters et al. 2009;
159 Singh et al. 2011; Chukwurah et al. 2021). To evaluate if PACT functions as an activator of PKR
160 in breast cancer cell lines, we overexpressed either wildtype PACT, or two phospho-site
161 mutants of PACT (phosphomimetic S287D and phospho-null S287A). Those mutants alter a
162 serine residue in PACT that was previously shown to enhance activation of PKR when
163 phosphorylated (Peters et al. 2009; Singh et al. 2011). Overexpression of neither PACT,
164 PACT^{S287D} nor PACT^{S287A} had any effect on PKR activation (phosphorylation of PKR on Thr-
165 446) in four different TNBC cell lines (Fig. 3a-b). To further evaluate if PACT functions as an
166 activator of PKR in cancer, we compared PACT expression at the protein level with expression
167 of ATF4, a component of the ISR that is induced upon PKR activation (Costa-Mattioli and Walter
168 2020). We observed no correlation between PACT and ATF4 protein expression across cancer
169 cell lines for which proteomic data were available (Fig. 3c). As a control, we compared ATF4
170 expression to ATF3, a transcription factor induced by ATF4, and found a strong correlation (Fig.
171 3d). Together these findings do not support PACT functioning as a PKR activator.

172 **PACT suppresses PKR activation, but not activation of other dsRNA sensors**

173 To further evaluate the role of PACT in TNBC cell lines, we used CRISPR-Cas9 to
174 deplete PACT in a panel of PACT-dependent and PACT-independent cell lines (Fig. 4a-b). The
175 PACT-dependent and -independent cell lines chosen are also ADAR1-dependent and -
176 independent, respectively (Fig. 4a). Consistent with DepMap data, for PACT-dependent cell

177 lines, depletion of PACT reduced cell viability, but in PACT-independent cell lines, depletion of
178 PACT had no effect on viability as measured by an ATP dependent luciferase activity (Fig. 4c).
179 For two PACT-dependent cell lines, we further evaluated the effect of PACT depletion on cell
180 viability and proliferation by crystal violet staining. Depletion of PACT reduced crystal violet
181 stained foci in both HCC1806 and MDA-MB-468 (Fig. 4d). To evaluate the *in vivo* effect of
182 PACT depletion on tumorigenesis, we performed an orthotopic xenograft study with inducible
183 knockout of PACT in HCC1806 cells. Tumorigenesis was significantly reduced by PACT
184 depletion, highlighting the potential of targeting PACT to treat TNBC (Fig. 4e).

185 In PACT-dependent cell lines, but not PACT-independent cell lines, depletion of PACT
186 caused activation of PKR (Fig. 4b,f). This finding suggests that PACT functions not as an
187 activator of PKR, but as a suppressor of PKR activation. We performed RNA-seq on PACT
188 depleted and control HCC1806 and MDA-MB-468 cells to evaluate transcriptomic response to
189 PACT depletion (Fig. 5a-b, Supplemental Tables 3-4). Activation of the dsRNA sensors MDA5,
190 RIG-I and TLR3 leads to induction of type I IFN stimulated genes (ISG) (Matsumoto et al. 2011;
191 Rehwinkel and Gack 2020). PACT depletion had little effect on type I ISG (Hallmark interferon
192 alpha response (Liberzon et al. 2015)) expression in HCC1806 or MDA-MB-468 (Fig. 5c;
193 Supplemental Fig. S3a-b). This observation was validated by qRT-PCR which again indicated
194 little to no change in ISG expression in PACT depleted cells relative to controls, except for one
195 ISG (IFIT2) which was elevated in the PACT-independent cell line MDA-MB-453 upon PACT
196 depletion (Fig. 5d). The 2'-5'-oligoadenylate synthases (OAS1, OAS2, and OAS3) are another
197 group of dsRNA sensors that are also ISGs (Hovanessian and Justesen 2007). When activated,
198 the OAS proteins activate RNase L which degrades many cellular RNAs, including rRNA leaving
199 behind a distinctive banding pattern (Chakrabarti et al. 2011). Analysis of rRNA integrity in
200 PACT-depleted and control cells revealed no cleavage that would be consistent with RNase L
201 activation (Fig. 5e). Taken together, these findings suggest that in PACT-dependent cells, PACT
202 suppresses activation of PKR, but not MDA5, RIG-I, TLR3 or the OASs.

203 **Activation of PKR in PACT depleted cells drives cell death and activation of ISR and NF-**
204 **κB**

205 Gene set enrichment analysis of PACT depleted cells identified many dysregulated
206 pathways. The top two most upregulated pathways in both HCC1806 and MDA-MB468 were
207 associated with NF-κB signaling (Hallmark TNFA signaling via NFKB (Liberzon et al. 2015)) and
208 the ISR (ATF4 target genes (Wong et al. 2019)). PKR is a well-known activator of the ISR,
209 which is largely facilitated by the transcription factor ATF4 (Gal-Ben-Ari et al. 2018; Costa-
210 Mattioli and Walter 2020). In PACT-depleted cells, we observed elevated expression of several
211 ATF4 targets, consistent with activation of ISR, in both our RNA-seq data, (Fig. 6a;
212 Supplemental Fig. S3c-d,g; Supplemental Tables 7-8) and by qRT-PCR (Fig. 6b). Immunoblot
213 analysis confirmed upregulation of the ATF4 targets GADD34 (encoded by *PPP1R15A*) and
214 ATF3 (Fig. 6d; Supplemental Fig. 3i). We did not observe robust phosphorylation of eIF2α as
215 would be expected based on the ISR signature in our RNA-seq data and activation of PKR (Fig.
216 6d; Supplemental Fig. 3i). However, GADD34, an eIF2α phosphatase that is expressed during
217 the ISR to dephosphorylate eIF2α to shut down the ISR (Novoa et al. 2001) was highly
218 expressed in our cells at the time of harvest which could explain the lack of elevated p-eIF2α in
219 PACT depleted cells (Fig. 6d).

220 In addition to the ISR, PKR can also activate the transcription factor NF-κB (Kumar et al.
221 1994; Gil et al. 1999; Bonnet et al. 2000; Zamanian-Daryoush et al. 2000; Gil et al. 2001;
222 Bonnet et al. 2006; Chukwurah et al. 2021). Multiple NF-κB targets were upregulated upon
223 PACT depletion in PACT-dependent cell lines as assessed by RNA-seq (Fig. 6a; Supplemental
224 Fig. S3e-f,h; Supplemental Tables 7-8), and qRT-PCR (Fig. 6c). Immunoblot confirmed
225 phosphorylation of NF-κB p65 (Ser468) in PACT depleted HCC1806 cells (Fig. 6d). Given that
226 PKR activation can drive cell death, we performed a combined depletion experiment to
227 determine if PKR activation is required for cell death upon PACT depletion (Fig. 6e). Depletion
228 of PKR by CRISPR-Cas9 completely rescued the reduced viability caused by depletion of PACT

229 in the PACT-dependent cell line HCC1806 (Fig. 6f). Furthermore, in PKR depleted cells,
230 depletion of PACT did not cause activation of ATF4 or NF- κ B target genes (Fig. 6g), indicating
231 that elevated ATF4 and NF- κ B target gene expression in PACT depleted cells is entirely
232 dependent on PKR activation.

233 **PACT requires dimerization and dsRNA binding to suppress PKR activation**

234 Multiple proteins suppress activation of PKR through binding to endogenous dsRNAs
235 (Park et al. 1994; Elbarbary et al. 2013; Hu et al. 2023; Cottrell et al. 2024b). For instance, while
236 ADAR1 prevents activation of MDA5 through A-to-I editing, it suppresses PKR activation
237 through competition for dsRNA binding via its dsRBDs (Hu et al. 2023). To determine if dsRNA
238 binding by PACT is required to suppress PKR activation, we performed a rescue experiment in
239 which we overexpressed either wildtype PACT, or two dsRNA binding mutants of PACT. The
240 mutants chosen, PACT-AA and PACT-EAA, were based on previous studies of PACT and
241 ADAR1, in which two or three lysines of the KKxAK motif within their functional dsRBDs (the
242 third dsRBD of PACT does not bind dsRNA (Peters et al. 2001)) had been mutated to abolish
243 dsRNA binding (Valente and Nishikura 2007; Takahashi et al. 2013) (Fig. 7a). For both the
244 wildtype and PACT mutants, we made synonymous mutations in the PACT coding sequence to
245 prevent sgRNA binding. Depletion of PACT in empty vector (EV) control cells caused activation
246 of PKR and reduced viability as before (Fig. 7b-d). Both phenotypes were completely rescued
247 by overexpression of wildtype PACT, but neither of the PACT dsRNA binding mutants rescued,
248 indicating that PACT suppresses PKR activation through binding endogenous dsRNAs (Fig. 7b-
249 d).

250 Like PKR, PACT forms a homodimer, which is facilitated by its third dsRBD (Heyam et
251 al. 2017). To evaluate if dimerization of PACT is required for its ability to suppress PKR
252 activation, we performed another knockout-rescue experiment with two different PACT
253 constructs. For the first construct, PACT^{Δd3}, we truncated PACT to remove its third dsRBD,
254 which is required for PACT dimerization (Heyam et al. 2017). To orthogonally restore

255 dimerization of PACT^{Δd3}, we generated a fusion construct that contained truncated PACT fused
256 to GST to generate PACT^{Δd3}-GST (Fig. 7e). As GST forms a strong dimer, this construct would
257 be expected to restore dimerization of PACT^{Δd3}. Like WT PACT, PACT^{Δd3} and PACT^{Δd3}-GST
258 maintained cytoplasmic localization (Supplemental Fig. 4a). When expressed in PACT depleted
259 cells, PACT^{Δd3} did not rescue PKR activation or fully rescue cell viability (Fig. 7f-h). Conversely,
260 PACT^{Δd3}-GST completely rescued both PKR activation and cell viability (Fig. 7f-h), as well as
261 ISR and NF-κB activation (Supplemental Fig. 4b). These findings indicate that while dsRBD3 is
262 required for suppression of PKR activation, its function regarding suppression of PKR activation
263 is only to allow for dimerization of PACT – which is required to suppress PKR activation.

264 **PACT and ADAR1 redundantly suppress PKR activation in PACT/ADAR1-independent** 265 **cell lines**

266 Given that PACT and ADAR1 are co-dependent genes in many cancer cell lines, and
267 that they both rely on dsRNA binding to suppress PKR activation, we hypothesized that
268 depletion of both ADAR1 and PACT in a PACT/ADAR1-independent cell line would cause
269 activation of PKR. To evaluate that hypothesis, we depleted both PACT and ADAR1, each
270 individually, or neither, in two PACT/ADAR1-independent TNBC cell lines, BT-549 and MDA-
271 MB-453. As in our previous experiments, depletion of PACT alone in both cell lines had little to
272 no effect on cell viability or PKR activation, and we observed the same for depletion of ADAR1
273 (Fig. 8a-c). Conversely, combined depletion of both ADAR1 and PACT in both cell lines caused
274 robust activation of PKR and for BT-549 reduced viability. Consistent with PKR activation, we
275 observed increased expression of ATF4 targets only in the PACT and ADAR1 depleted cells
276 (Fig. 8d). Unlike in PACT-dependent cell lines, we did not observe substantial changes in NF-κB
277 target expression (Fig. 8e). While the expression of most ISGs evaluated remained unchanged
278 upon depletion of PACT and/or ADAR1 in each cell line, the ISG IFIT2 was upregulated upon
279 PACT depletion in MDA-MB-453 and was further induced in the combined depleted cells (Fig.

280 8f). Finally, we observed no rRNA degradation consistent with OAS/RNase L activation upon
281 depletion of PACT and/or ADAR1 in either cell line (Fig. 8g).

282 To further evaluate redundancy between PACT and ADAR1, we attempted to rescue the
283 effects of PACT depletion in PACT-dependent cells by overexpression of each isoform of
284 ADAR1. Overexpression of either the p110 or p150 isoform of ADAR1 partially rescued PKR
285 activation and reduced viability caused by depletion of PACT in HCC1806 cells (Fig. 8h-j).
286 Taken together with the combined depletion experiments above, these data support a
287 redundant role for PACT and ADAR1 in suppression of PKR activation in PACT/ADAR1-
288 independent cell lines.

289 **PACT-dependency correlates with PKR expression, which is elevated in TNBC**

290 While the data above provide strong evidence to support PACT as a suppressor of PKR
291 activation, they do not explain the differential sensitivity of PACT-dependent and PACT-
292 independent cell lines to depletion of PACT. For ADAR1-dependency, it has been proposed that
293 chronic IFN signaling in ADAR1-dependent cells, which drives elevated expression of the
294 dsRNA sensors MDA5, RIG-I, PKR and the OASs, sensitizes those cells to depletion of ADAR1
295 (Liu et al. 2019). This model likely does not explain PACT-dependency, because unlike ADAR1-
296 dependency, there is no correlation between PACT-dependency score and ISG expression (Fig.
297 9a-b; Supplemental Fig. S5a-b). By analyzing proteomics data for cancer cell lines, we found
298 that PACT-dependency strongly correlates with PKR expression at the protein level (Fig. 9c and
299 Supplemental Fig. S5c-g). The correlation between PACT-dependency score and PKR protein
300 expression is strongest in breast cancer (Fig. 9d). Consistent with the proteomics and DepMap
301 data, we observed higher PKR expression in PACT-dependent cells relative to PACT-
302 independent cells (Fig. 9e). Based on mass-spectrometry data, PKR expression is highest in
303 TNBC cell lines (Fig. 9f) and in human tumors, PKR expression at the RNA level is elevated in
304 breast tumors relative to normal breast, with TNBC tumors generally having higher expression
305 (Fig. 9g-h; Supplemental Fig. S5h-i). While not as predictive as PKR expression, it should be

306 noted that the expression of PACT itself correlates with PACT-dependency score (Supplemental
307 Fig. S5j-m).

308 **Discussion**

309 The role of PACT in regulation of PKR has been controversial in the literature. Early
310 reports, which gave PACT its name, provided compelling evidence that PACT functioned to
311 activate PKR through protein-protein interactions in the absence of dsRNA (Patel and Sen
312 1998; Peters et al. 2001; Li et al. 2006; Peters et al. 2009). Many groups have reported similar
313 findings, often with PACT functioning to activate PKR during stress (Patel et al. 2000; Singh et
314 al. 2011; Farabaugh et al. 2020; Chukwurah et al. 2021). However, other studies indicated that
315 PACT conducts the exact opposite function, inhibiting PKR, including a mouse study showing
316 that PKR (*Eif2ak2*) knockout could rescue embryonic lethality of PACT (Rax in mice, *Prkra*)
317 knockout (Clerzius et al. 2013; Dickerman et al. 2015; Meyer et al. 2018). During the
318 preparation of this manuscript, two studies were published that provided more definitive
319 evidence, consistent with our data here, in support of PACT's role as a suppressor of PKR
320 activation (Ahmad et al. 2025; Manjunath et al. 2025).

321 While our data indicate that PACT suppresses PKR activation through dimerization and
322 dsRNA binding, the finer details of the mechanism are not clear from our work alone.
323 Fortunately, another group has examined the mechanism and reported those findings during the
324 preparation of this manuscript (Ahmad et al. 2025). In this work, Ahmad, Zou, and Xhao et al.,
325 reveal that PACT suppresses PKR activation by preventing dimerization of sliding PKR
326 monomers. Specifically, they propose a model in which weak protein-protein interactions
327 between PKR and PACT prevent sliding of PKR along dsRNA thus preventing monomers from
328 colliding and forming an active PKR dimer. While that model is supported by our own data
329 showing that PACT requires dsRNA binding to prevent PKR activation, it is not clear how
330 dimerization of PACT fits into the model. A recent study, published during the preparation of this
331 manuscript, found that dimerization of the zebrafish homologue of PACT (*Prkra*) facilitated

332 binding to and inhibition of eIF2 (Lu et al. 2025). In the model presented with those findings,
333 Prkra uses its third dsRBD to dimerize and sequester eIF2 to inhibit translation, thus assigning a
334 dual role for dsRBD3. Here, we found that dsRBD3 of PACT can be functionally replaced by
335 GST (a dimeric protein), indicating that at least in human cells, dsRBD3's only function in
336 relation to suppression of PKR activity is to facilitate dimerization of PACT. How dimerization
337 enables PKR inhibition is unclear. It is unlikely that dimerization allows PACT to better 'compete'
338 with PKR for binding dsRNA as PACT mutants lacking the third dsRBD bind a model dsRNA
339 with the same affinity as full-length PACT (Ahmad et al. 2025). Structural studies are needed to
340 understand the role of dimerization; perhaps dimerization exposes the PKR binding site on
341 PACT, or allows for higher-order structures of PACT-PKR-dsRNA that inhibit or sequester PKR.

342 Based on the elevated expression of PKR in PACT-dependent cells, we propose a
343 model in which PACT-dependent cells are in a poised state, where because of the elevated
344 abundance of PKR, the cell is highly sensitive to depletion of PACT, and in many cases ADAR1
345 (Fig. 9i). Conversely, in PACT-independent cell lines, the lower expression of PKR enables
346 either PACT or ADAR1 alone to suppress PKR activation. In these cells, PACT and ADAR1 are
347 functioning redundantly. This shared role of PACT and ADAR1 was also reported in a recent
348 study published during preparation of this manuscript (Manjunath et al. 2025). This redundancy
349 between ADAR1 and PACT is not unique. We have observed the same paradigm before for
350 DHX9 and ADAR1, where depletion of DHX9 in ADAR1-dependent cells causes activation of
351 PKR, while in ADAR1-independent cells, DHX9 and ADAR1 function redundantly to suppress
352 activation of PKR and other dsRNA sensors (Cottrell et al. 2024b). A common thread
353 connecting these proteins is the presence of dsRBDs. Here we show that the dsRNA binding
354 activity of PACT is required for suppression of PKR activation, the same has been observed for
355 ADAR1 previously (Hu et al. 2023), and for DHX9 expression of its dsRBDs alone is sufficient to
356 suppress PKR activation (Cottrell et al. 2024b). While previous cellular studies indicate that
357 ADAR1 suppresses PKR activation by competing with PKR for dsRNA binding, but the same

358 was not observed *in vitro* by Ahmad, Zou, and Xhao et al. (Hu et al. 2023; Ahmad et al. 2025).
359 Further studies are needed to evaluate in finer detail the mechanism by which ADAR1
360 suppresses PKR activation, and how that may or may not differ from PACT. More research is
361 also needed to understand the role of ADAR1-p110 in suppressing PKR activation. Previous
362 literature supports p150 as the ADAR1 isoform that suppresses PKR activation (Chung et al.
363 2018; Hu et al. 2023), though here we show that overexpression of p110 in PACT depleted cells
364 reduces PKR activation. We have observed something similar in DHX9 and ADAR1 depleted
365 cells, where expression of p110 was capable of suppressing PKR activation (Cottrell et al.
366 2024b). Additionally, Sinigaglia et al. observed reduced PKR activation upon p110
367 overexpression in A549 cells (Sinigaglia et al. 2024). In that study, a different model for
368 inhibition of PKR by ADAR1 is proposed, a model in which the third dsRBD of ADAR1 binds the
369 kinase domain of PKR preventing its activation. It is of course possible that suppression of PKR
370 by p110 in these contexts is an artifact of overexpression and does not occur physiologically. Or
371 perhaps, p110 utilizes this function in specific contexts when p150 or other proteins are
372 unavailable, possibly in the nucleus (to which some PKR localizes, Supplemental Fig. S4a)
373 (Jeffrey et al. 1995) or during mitosis, during which nuclear RNAs can activate PKR (Kim et al.
374 2014).

375 Finally, here we provide strong evidence to support the therapeutic targeting of PACT to
376 treat TNBC. There are several attributes that make PACT a good target for TNBC, 1) PACT is
377 highly expressed in TNBC, 2) PACT is essential in many TNBC cell lines, 3) PKR expression,
378 which correlates with PACT-dependency, is elevated in TNBC. While PACT has no known
379 enzymatic functions, disrupting PACT dimerization would inhibit its regulation of PKR. As such,
380 PACT dimerization inhibitors, or PACT degraders, could have therapeutic potential for TNBC,
381 and likely many other types of cancer.

382 **Materials and Methods**

383 **Cell culture**

384 Cell lines (MCF-7 (RRID:CVCL_0031), SK-BR-3 (RRID:CVCL_0033), BT-549 (RRID:
385 CVCL_1092), HCC1806 (RRID: CVCL_1258), MDA-MB-468 (RRID: CVCL_0063) MDA-MB-453
386 (RRID: CVCL_0418), and 293T (RRID: CVCL_0063) were obtained from American Type
387 Culture Collection which used STR profiling to authenticate the cell lines, all cell lines were
388 obtained between 2023 and 2024. The cell lines 293T and SK-BR-3 were cultured in Dulbecco's
389 modified Eagle's medium (DMEM) (Hyclone) with 10% fetal bovine serum (BioTechne), 2 mM
390 glutamine (Hyclone), 0.1 mM nonessential amino acids (Hyclone), and 1 mM sodium pyruvate
391 (Hyclone). The cell lines MDA-MB-453 and MDA-MB-468 were cultured in Leibowitz L-15 media
392 (HyClone Cat# SH30525) with 10% fetal bovine serum (BioTechne). The cell lines HCC1806
393 and BT-549 were cultured in Roswell Park Memorial Institute 1640 media (Corning Cat# 10-
394 041-CV) with 10% fetal bovine serum (BioTechne), for BT-549 recombinant insulin (Gibco) was
395 added to 0.78 µg/mL. The cell line MCF-7 was cultured in modified Eagle's media (HyClone
396 Cat# SH30024.01) with 10% fetal bovine serum (BioTechne) and recombinant insulin at 10.2
397 µg/mL. Except for MDA-MB-453 and MDA-MB-468, all cell lines were grown at 37 °C at 5%
398 CO₂, MDA-MB-453 and MDA-MB-468 were grown at 37 °C with atmospheric CO₂. Mycoplasma
399 testing was performed by a PCR based method. All experiments were performed with cells
400 under twenty passages.

401 **Viral Production and Transduction**

402 Lentivirus was produced by LipoFexin (Lamda Biotech) or Polyethylenimine (branched,
403 ~25,000 Da, Sigma-Aldrich) transfection of 293T cells with pCMV-VSV-G (a gift from Bob
404 Weinberg (Stewart et al. 2003), Addgene plasmid #8454; RRID:Addgene_8454) or pMD2.G (a
405 gift from Didier Trono, Addgene plasmid #12259; RRID:Addgene_12259) and pSPAX2 (a gift
406 from Didier Trono, Addgene plasmid #12260; RRID:Addgene_12260), and a transfer plasmid for
407 expression of genes of interest, shRNAs, or sgRNAs. Culture media was changed the day after
408 transfection and lentivirus containing media was collected the following day, or after two days.
409 Lentivirus containing media was filtered through a 0.45 µm filter before transduction of cells of

410 interest in the presence of 10 µg/mL protamine sulfate (Sigma-Aldrich). Depending on the
411 transfer plasmid used and cell line, cells were selected with puromycin at 2 µg/mL (Sigma-
412 Aldrich), 150 µg/mL hygromycin (Gibco or InvivoGen) 10 µg/mL Blasticidin (Fisher or
413 InvivoGen), or 500 µg/mL G418 (InvivoGen).

414 **Plasmids**

415 For all sgRNAs targeting genes of interest, oligos encoding the sgRNAs (Supplemental
416 Table 1) were cloned into lentiGuide-puro (a gift from Feng Zhang ⁴⁴, Addgene #52961;
417 RRID:Addgene_52963), lenti-sgRNA-hygro (a gift from Brett Stringer (Stringer et al. 2019),
418 Addgene #104991; RRID:Addgene_104991), or tet-pLKO-sgRNA-puro (a gift from Nathanael
419 Gray (Huang et al. 2017), Addgene plasmid # 104321; RRID:Addgene_104321) by ligation of
420 annealed and phosphorylated oligos into a restriction enzyme digested and dephosphorylated
421 vector. The sgRNA sequence for lenti-sgPKR-hygro was used previously (Zou et al. 2024). The
422 pLKO-shSCR-hygro and pLKO-shADAR1-hygro plasmids have been described previously
423 (Cottrell et al. 2024b).

424 Two control sgRNAs were used in this study. One (sgC1) targets a control genomic
425 locus (AAVS1) and has been used previously (Zou et al. 2024). The second control sgRNA
426 (sgNTA) is a non-targeting sgRNA described previously (Doench et al. 2016). For sgNTA,
427 lentiGuide-sgNTA-puro was purchased from Addgene (a gift from John Doench & David Root
428 (Doench et al. 2016), Addgene plasmid #80248; RRID:Addgene_80248). All other plasmids for
429 the control sgRNAs were cloned in the same manner as described above, and all sequences
430 are available in Supplementary Table 1.

431 The PACT coding sequence flanked by BamHI and MluI restriction enzyme sites, a
432 Kozak sequence (5'-CACC-3'), and containing wobble mutations to prevent targeting of sgRNAs
433 was synthesized by TwistBio. Restriction enzyme digest and ligation was used to clone PACT
434 into pLV-EF1a-IRES-Blast vector (a gift from Tobias Meyer ⁴⁵, Addgene plasmid #85133;
435 RRID:Addgene_85133). The PACT dsRBD mutants were cloned in the same manner, all coding

436 sequences can be found in the Supplemental Information. The PACT-dsRBD3 constructs were
437 made through restriction enzyme digest and ligation. For the PACT^{Δd3} plasmid, pLV-EF1a-
438 PACT-IRES-Blast was digested with EcoRI, which cuts between the coding sequence for
439 dsRBD2 and dsRBD3 within PACT, and 3' of PACT within pLV-EF1a-IRES-Blast. A short
440 double-stranded DNA oligonucleotide encoding two stop codons was ligated in frame with the
441 PACT coding sequence to generate pLV-EF1a- PACT^{Δd3}-IRES-Blast. The plasmid for PACT^{Δd3}-
442 GST was cloned in the same manner with GST in place of the oligonucleotide insert. GST was
443 PCR amplified from pDEST15, kindly provided by Dr. Mark Hall, Purdue University. The PCR
444 primers and oligonucleotides used for cloning the PACT-dsRBD3 constructs, as well as the
445 coding sequences of the final constructs can be found in Supplementary Table 1 and the
446 Supplemental Information. The ADAR1 overexpression constructs used here (pLV-EF1-Blast-
447 p110 and pLV-EF1-Blast-p150) were cloned previously (Cottrell et al. 2024b).

448 All plasmids were confirmed by restriction enzyme digest, as well as Sanger sequencing
449 and Nanopore whole plasmid sequencing.

450 **Genetic Depletion by CRISPR-Cas9**

451 For all CRISPR-Cas9 depletion experiments, the cell lines used in this study were
452 transduced with lentivirus for inducible expression of Cas9 (iCas9) using the transfer plasmid
453 lenti-iCas9-neo (a gift from Qin Yan (Cao et al. 2016), Addgene plasmid # 85400;
454 RRID:Addgene_85400). After transduction and selection with G418, cells with high GFP
455 expression upon doxycycline induction were sorted on a BD FACS Aria by the Purdue Flow
456 Cytometry and Cell Separation Facility. We used either constitutively expressed or inducible
457 sgRNAs targeting genes of interest. For constitutively expressed sgRNAs, we observed
458 premature knockout of the genes of interest in uninduced cells, likely due to 'leaky' expression
459 of Cas9. As such, for all experiments utilizing constitutive sgRNA expression (single knockout of
460 PACT in Fig. 4, or combined knockout of PACT and knockdown of ADAR1 in Fig. 8), we began
461 each biological replicate by transducing cells with the lentivirus for sgRNA expression followed

462 by selection and induction with doxycycline. The timelines for transduction, selection, induction,
463 harvesting of cells and evaluation of cell viability for each cell line is described in Supplemental
464 Table 2.

465 For all knockout-rescue experiments and combined knockout of PACT and PKR, we
466 combined iCas9 with an inducible sgRNA construct (tet-pLKO-sgRNA-puro) which prevented
467 knockout prior to induction (data not shown). PACT overexpression and empty vector (EV)
468 control HCC1806-iCas9 cells were generated by lentiviral transduction and selection for
469 transgene incorporation with blasticidin. Subsequently, PACT overexpression and control EV
470 HCC1806-iCas9 lines were transduced with lentivirus made with tet-pLKO-sgPACT-2-puro or
471 tet-pLKO-sgNTA-puro and selected with puromycin. Experimental replicates were initiated by
472 doxycycline treatment and the timeline is described in Supplemental Table 2. For PKR
473 knockout, HCC1806-iCas9 cells were first transduced with lentivirus made with lenti-sgC1-
474 hygro, lenti-sgPKR-1-hygro or lenti-sgPKR-2-hygro and selected with hygromycin. Cas9
475 expression was induced by doxycycline and PKR knockout was confirmed by immunoblot (data
476 not shown). The HCC1806-iCas9 control and PKR knockout lines were passaged without
477 doxycycline before transduction with lentivirus made with tet-pLKO-sgPACT-2-puro or tet-pLKO-
478 sgNTA-puro and selected with puromycin. Experimental replicates were initiated by doxycycline
479 treatment and the timeline is described in Supplemental Table 2.

480 **Immunoblot**

481 Cell pellets were lysed and sonicated in RIPA Buffer (50 mM Tris pH 7.4 (Ambion), 150
482 mM NaCl (Ambion), 1% Triton X-100 (Sigma-Aldrich), 0.1% sodium dodecyl sulfate (Promega)
483 and 0.5% sodium deoxycholate (Sigma-Aldrich) with 1x HALT Protease and Phosphatase
484 Inhibitor (Pierce). The DC Assay kit (Bio-Rad) was used to quantify protein concentration. The
485 lysate was diluted in SDS Sample Buffer (125 mM Tris pH 6.8, 30% glycerol, 10% sodium
486 dodecyl sulfate, 0.012% bromophenol blue) and denatured at 95 °C for 7 minutes. Between 20
487 and 40 micrograms of total protein was loaded per lane of 4-12% TGX Acrylamide Stain-Free

488 gels (Bio-Rad). Prior to transfer by TransBlot Turbo (Bio-Rad), the Stain-Free gel was imaged to
489 quantify total protein (Millipore or Bio-Rad). Blots were blocked in 5% milk or 5% bovine serum
490 albumin in tris-buffered saline with tween prior to adding primary antibody: ADAR1 (Santa Cruz
491 Biotechnology Cat# sc-73408, RRID:AB_2222767; Bethyl Cat# A303-883A,
492 RRID:AB_2620233), ATF3 (Cell Signaling Technology Cat# 33593, RRID:AB_2799039), eIF2a
493 (Abcam Cat# ab5369, RRID:AB_304838), eIF2a-Ser-51-P (Abcam Cat# ab32157,
494 RRID:AB_732117), Phospho-NF- κ B p65 (Ser 468) (Cell Signaling Technology Cat# 3039S,
495 RRID:AB_330579), NF- κ B p65 (Cell Signaling Technology Cat# 8242S, RRID:AB_10859369),
496 beta-tubulin (Abcam Cat# ab6046, RRID:AB_2210370), cleaved PARP (Cell Signaling
497 Technology Cat# 9541, RRID:AB_331426), GADD34 (Cell Signaling Technology Cat# 41222),
498 Histone H3 (Abcam Cat# 10799, RRID:AB_470239), PACT (Cell Signaling Technology Cat#
499 13490, RRID AB_2798233), PKR (Cell Signaling Technology Cat# 3072, RRID:AB_2277600),
500 PKR Thr-446-P (Abcam Cat# ab32036, RRID:AB_777310). Horseradish-peroxidase conjugated
501 secondary antibodies (Jackson ImmunoResearch) and Clarity Western ECL Substrate (Bio-
502 Rad) were used for detection via ChemiDoc (Bio-Rad). Image Lab (Bio-Rad) was used to
503 determine band intensities which were normalized to total protein measured by imaging of the
504 Stain-Free gel.

505 **Cell Viability and Crystal Violet Staining**

506 For cell viability assessment, 5000 cells were plated in triplicate for each condition in
507 opaque white 96-well plates. Cell viability was assessed by CellTiter-Glo 2.0 (Promega) per
508 manufacturers protocol between three and four days after plating. For details on the number of
509 cells plated and the timeline for cell viability assessment, see Supplemental Table 2.

510 For crystal violet staining, 2000 cells were plated per well of a 6-well dish. Between 15 to
511 20 days later, cells were washed briefly with 1x PBS prior to fixation in 100% methanol for 5
512 min. After drying, the cells were stained with 0.005% Crystal Violet solution containing 25%

513 methanol (Sigma-Aldrich) prior to washing excess stain away with deionized water. Plates were
514 imaged using a Bio-Rad ChemiDoc.

515 **Tumorigenesis**

516 The Biological Evaluation Shared Resource at Purdue University Institute for Cancer
517 research performed the tumorigenesis study. From the cranial end, the second left ventral
518 mammary fat-pad of female NRG (NOD.Cg-Rag1tm1Mom Il2rgtm1Wjl/SzJ) mice, originally
519 obtained from The Jackson Laboratory (RRID:IMSR_JAX:007799), were injected with 2.9×10^6
520 HCC1806 cells suspended in equal volumes 1X PBS and Matrigel (Corning). Five days after
521 injection, when tumors were palpable, mice were given acidified drinking water containing 2.4
522 mg/mL doxycycline. Tumor volume was measured manually using a caliper three days per week
523 until the first mouse reached a humane euthanasia criterion. Five mice were injected per
524 condition, one mouse injected with the sgNTA line was euthanized early due to poor health.

525 **RNA Purification and Analysis of rRNA Integrity**

526 RNA was purified using the Nucleospin RNA kit (Macherey-Nagel). Ribosomal RNA
527 integrity was determined using an Agilent TapeStation by the Genomics and Genome Editing
528 Facility at Purdue University.

529 **RNA Sequencing and Analysis**

530 Contaminating DNA was removed from total RNA by TURBO DNase (Thermo Fisher
531 Scientific) prior to rRNA depletion using QIAseq® FastSelect™-rRNA HMR kit (Qiagen) per
532 manufacturer's protocol. RNA sequencing libraries were constructed with the NEBNext Ultra II
533 RNA Library Preparation Kit for Illumina per manufacturer's recommendations. Sequencing
534 libraries were validated by Agilent TapeStation 4200 and quantified by Qubit 2.0 Fluorometer
535 (ThermoFisher Scientific) as well as by quantitative PCR (KAPA Biosystems). The sequencing
536 libraries were multiplexed and clustered onto a flowcell on the Illumina NovaSeq instrument.
537 The samples were sequenced using a 2x150bp paired-end configuration. Image analysis and
538 base calling were conducted by NovaSeq Control Software. Raw sequence data (.bcl files)

539 generated from Illumina NovaSeq was converted into fastq files and de-multiplexed using
540 Illumina bcl2fastq 2.20 software. One mismatch was allowed for index sequence identification.
541 Sequence reads were processed using Trimmomatic v.0.36 to remove adapter
542 sequences and poor-quality nucleotides. Trimmed reads were aligned to GRCh38 reference
543 genome using STAR aligner v2.5.2b (RRID:SCR_004463). Gene counts were determined using
544 featureCounts from Subread v.1.5.2 (RRID:SCR_009803), only unique exonic reads were
545 counted. Differential gene expression was determined using DESeq2 (RRID:SCR_015687, see
546 Data Availability below for scripts) with shrunken fold changes using the 'apeglm' method ⁴⁹.
547 Gene set enrichment analysis was performed using 'clusterProfiler' (RRID:SCR_016884) with
548 Gene Ontology (RRID:SCR_002811) terms from (Ashburner et al. 2000; Aleksander et al.
549 2023) or Hallmark gene sets from the Molecular Signatures Database (RRID:SCR_016863)
550 (Liberzon et al. 2015). For Gene Set Enrichment Analysis with Hallmark gene sets, an additional
551 gene set was included for previously identified ATF4 target genes (Wong et al. 2019).

552 **Quantitative PCR**

553 LunaScript Supermix (NEB) was used to make cDNA for quantitative PCR (qPCR),
554 using Luna Universal qPCR MasterMix (NEB) on a QuantStudio3 system (Thermo Scientific).
555 All primers used for qPCR are listed in Supplemental Table 1. The amplification efficiency of
556 each primer was verified to be within 90-110% allowing determination of 'Fold Change' by the
557 $\Delta\Delta C_t$. Two reference genes were used for normalization, EEF1A1 and HSPA5, using their
558 geometric mean Ct for calculating ΔC_t .

559 **Analysis of TCGA data**

560 For TCGA data, normalization of RNA-seq data, and z-scores calculations were
561 performed as previously described ³⁵. Breast cancer cell lines and TCGA tumor molecular
562 subtypes were defined previously ⁵³. The R packages RTCGA and survminer
563 (RRID:SCR_021094) were used to determine breast cancer survival ^{54,55}. The surv_cutpoint
564 function of survminer was employed to determine an expression cutoff.

565 **Data Availability Statement**

566 All analysis scripts are available at (https://github.com/cottrellka/Young_et_al_2025).

567 Raw RNA-seq and gene count data is available at the Gene Expression Omnibus

568 (GSE298233). Dependency (DepMap_Public_24Q4+Score,_Chronos, and

569 Achilles+DRIVE+Marcotte,_DEMETER2) , transcriptomic

570 (Batch_corrected_Expression_Public_24Q4) and proteomic data for cancer cell lines

571 (Harmonized_MS_CCLE_Gygi) were obtained from the DepMap portal

572 (<https://depmap.org/portal/download/custom/>, RRID:SCR_017655)⁵⁶. Transcriptomic data for

573 TCGA BRCA samples (illuminahisecq_rnaseqv2-RSEM_genes) and clinical data

574 (Merge_Clinical) were obtained from the Broad Institute FireBrowse and are available at

575 <http://firebrowse.org/>.

576 **Acknowledgements:**

577 The data described here is in part based on data generated by the TCGA Research

578 Network: <https://www.cancer.gov/tcga>. This work was supported by R00MD016946 (K.A.

579 Cottrell), the Purdue Institute for Cancer Research (start-up funding, Robbers New Investigator

580 Award to K.A. Cottrell, and support for the Biological Evaluation Shared Resource) NIH grant

581 P30CA023168, and start-up funding from Purdue University Department of Biochemistry and

582 College of Agriculture. Jill Hutchcroft, director of the Flow Cytometry and Cell Separation Facility

583 at Purdue University for sorting iCas9 cell lines. Cottrell Lab rotation students Jolene Mach,

584 Geethma Lirushie, Nima Goodarzi, Ayomide Adebessin, Yalan Huo, Troy Sievertsen, Tommy

585 Sheeley and Reed Smith.

586 **Author Contributions**

587 K.A.C. and A.A.Y. conceived the project. K.A.C., A.A.Y. and B.D.E. designed the

588 experiments. A.A.Y., K.A.C., I.G.J., J.R.P., H.E.B., H.A.H., D.S.O., R.N.C., M.E.L., E.N.G.,

589 performed the experiments and/or provided materials. K.A.C, A.A.Y., I.G.J., J.R.P., H.E.B.

590 performed the data analysis. K.A.C., A.A.Y., and I.G.J. wrote the manuscript. All authors edited
591 the manuscript.

592 **Declaration of interests**

593 The authors declare no competing interests.

594 **References**

- 595 Ahmad S, Zou T, Hwang J, Zhao L, Wang X, Davydenko A, Buchumenski I, Zhuang P, Fishbein
596 AR, Capcha-Rodriguez D et al. 2025. PACT prevents aberrant activation of PKR by
597 endogenous dsRNA without sequestration. *Nat Commun* **16**: 3325.
- 598 Aleksander SA Balhoff J Carbon S Cherry JM Drabkin HJ Ebert D Feuermann M Gaudet P
599 Harris NL Hill DP et al. 2023. The Gene Ontology knowledgebase in 2023. *Genetics*
600 **224**.
- 601 Ashburner M, Ball CA, Blake JA, Botstein D, Butler H, Cherry JM, Davis AP, Dolinski K, Dwight
602 SS, Eppig JT et al. 2000. Gene ontology: tool for the unification of biology. The Gene
603 Ontology Consortium. *Nat Genet* **25**: 25-29.
- 604 Bass BL. 2024. Adenosine deaminases that act on RNA, then and now. *RNA* **30**: 521-529.
- 605 Bass BL, Weintraub H. 1988. An unwinding activity that covalently modifies its double-stranded
606 RNA substrate. *Cell* **55**: 1089-1098.
- 607 Bianchini G, Balko JM, Mayer IA, Sanders ME, Gianni L. 2016. Triple-negative breast cancer:
608 challenges and opportunities of a heterogeneous disease. *Nat Rev Clin Oncol* **13**: 674-
609 690.
- 610 Bonnet MC, Daurat C, Ottone C, Meurs EF. 2006. The N-terminus of PKR is responsible for the
611 activation of the NF-kappaB signaling pathway by interacting with the IKK complex. *Cell*
612 *Signal* **18**: 1865-1875.
- 613 Bonnet MC, Weil R, Dam E, Hovanessian AG, Meurs EF. 2000. PKR stimulates NF-kappaB
614 irrespective of its kinase function by interacting with the IkappaB kinase complex. *Mol*
615 *Cell Biol* **20**: 4532-4542.
- 616 Broad D. 2024a. DepMap 24Q2 Public.
617 -. 2024b. DepMap 24Q4 Public.
- 618 Cao J, Wu L, Zhang SM, Lu M, Cheung WK, Cai W, Gale M, Xu Q, Yan Q. 2016. An easy and
619 efficient inducible CRISPR/Cas9 platform with improved specificity for multiple gene
620 targeting. *Nucleic Acids Res* **44**: e149.
- 621 Chakrabarti A, Jha BK, Silverman RH. 2011. New insights into the role of RNase L in innate
622 immunity. *J Interferon Cytokine Res* **31**: 49-57.
- 623 Chen DS, Mellman I. 2017. Elements of cancer immunity and the cancer-immune set point.
624 *Nature* **541**: 321-330.
- 625 Chen R, Ishak CA, De Carvalho DD. 2021. Endogenous Retroelements and the Viral Mimicry
626 Response in Cancer Therapy and Cellular Homeostasis. *Cancer Discov* **11**: 2707-2725.
- 627 Chen YG, Hur S. 2022. Cellular origins of dsRNA, their recognition and consequences. *Nat Rev*
628 *Mol Cell Biol* **23**: 286-301.
- 629 Chukwurah E, Farabaugh KT, Guan BJ, Ramakrishnan P, Hatzoglou M. 2021. A tale of two
630 proteins: PACT and PKR and their roles in inflammation. *FEBS J* **288**: 6365-6391.
- 631 Chung H, Calis JJA, Wu X, Sun T, Yu Y, Sarbanes SL, Dao Thi VL, Shilvock AR, Hoffmann HH,
632 Rosenberg BR et al. 2018. Human ADAR1 Prevents Endogenous RNA from Triggering
633 Translational Shutdown. *Cell* **172**: 811-824.e814.
- 634 Clerzius G, Shaw E, Daher A, Burugu S, Gélinas JF, Ear T, Sinck L, Routy JP, Mouland AJ,
635 Patel RC et al. 2013. The PKR activator, PACT, becomes a PKR inhibitor during HIV-1
636 replication. *Retrovirology* **10**: 96.
- 637 Costa-Mattioli M, Walter P. 2020. The integrated stress response: From mechanism to disease.
638 *Science* **368**.
- 639 Cottrell KA, Andrews RJ, Bass BL. 2024a. The competitive landscape of the dsRNA world. *Mol*
640 *Cell* **84**: 107-119.
- 641 Cottrell KA, Ryu S, Pierce JR, Soto Torres L, Bohlin HE, Schab AM, Weber JD. 2024b.
642 Induction of Viral Mimicry Upon Loss of DHX9 and ADAR1 in Breast Cancer Cells.
643 *Cancer Res Commun* **4**: 986-1003.

- 644 Curigliano G, Goldhirsch A. 2011. The triple-negative subtype: new ideas for the poorest
645 prognosis breast cancer. *J Natl Cancer Inst Monogr* **2011**: 108-110.
- 646 Dempster JM, Rossen J, Kazachkova M, Pan J, Kugener G, Root DE, Tsherniak A. 2019.
647 Extracting Biological Insights from the Project Achilles Genome-Scale CRISPR Screens
648 in Cancer Cell Lines. *bioRxiv*: 720243.
- 649 Dickerman BK, White CL, Kessler PM, Sadler AJ, Williams BR, Sen GC. 2015. The protein
650 activator of protein kinase R, PACT/RAX, negatively regulates protein kinase R during
651 mouse anterior pituitary development. *FEBS J* **282**: 4766-4781.
- 652 Doench JG, Fusi N, Sullender M, Hegde M, Vaimberg EW, Donovan KF, Smith I, Tothova Z,
653 Wilen C, Orchard R et al. 2016. Optimized sgRNA design to maximize activity and
654 minimize off-target effects of CRISPR-Cas9. *Nat Biotechnol* **34**: 184-191.
- 655 Elbarbary RA, Li W, Tian B, Maquat LE. 2013. STAU1 binding 3' UTR IRAlus complements
656 nuclear retention to protect cells from PKR-mediated translational shutdown. *Genes Dev*
657 **27**: 1495-1510.
- 658 Farabaugh KT, Krokowski D, Guan BJ, Gao Z, Gao XH, Wu J, Jobava R, Ray G, de Jesus TJ,
659 Bianchi MG et al. 2020. PACT-mediated PKR activation acts as a hyperosmotic stress
660 intensity sensor weakening osmoadaptation and enhancing inflammation. *Elife* **9**.
- 661 Gal-Ben-Ari S, Barrera I, Ehrlich M, Rosenblum K. 2018. PKR: A Kinase to Remember. *Front*
662 *Mol Neurosci* **11**: 480.
- 663 Gannon HS, Zou T, Kiessling MK, Gao GF, Cai D, Choi PS, Ivan AP, Buchumenski I, Berger
664 AC, Goldstein JT et al. 2018. Identification of ADAR1 adenosine deaminase dependency
665 in a subset of cancer cells. *Nat Commun* **9**: 5450.
- 666 Gil J, Alcamí J, Esteban M. 1999. Induction of apoptosis by double-stranded-RNA-dependent
667 protein kinase (PKR) involves the alpha subunit of eukaryotic translation initiation factor
668 2 and NF-kappaB. *Mol Cell Biol* **19**: 4653-4663.
- 669 Gil J, Rullas J, García MA, Alcamí J, Esteban M. 2001. The catalytic activity of dsRNA-
670 dependent protein kinase, PKR, is required for NF-kappaB activation. *Oncogene* **20**:
671 385-394.
- 672 Guirguis AA, Ofir-Rosenfeld Y, Knezevic K, Blackaby W, Hardick D, Chan YC, Motazedian A,
673 Gillespie A, Vassiliadis D, Lam EYN et al. 2023. Inhibition of METTL3 Results in a Cell-
674 Intrinsic Interferon Response That Enhances Antitumor Immunity. *Cancer Discov* **13**:
675 2228-2247.
- 676 Heyam A, Coupland CE, Dégut C, Haley RA, Baxter NJ, Jakob L, Aguiar PM, Meister G,
677 Williamson MP, Lagos D et al. 2017. Conserved asymmetry underpins homodimerization
678 of Dicer-associated double-stranded RNA-binding proteins. *Nucleic Acids Res* **45**:
679 12577-12584.
- 680 Hovanessian AG, Justesen J. 2007. The human 2'-5'oligoadenylate synthetase family: unique
681 interferon-inducible enzymes catalyzing 2'-5' instead of 3'-5' phosphodiester bond
682 formation. *Biochimie* **89**: 779-788.
- 683 Hu SB, Heraud-Farlow J, Sun T, Liang Z, Goradia A, Taylor S, Walkley CR, Li JB. 2023.
684 ADAR1p150 prevents MDA5 and PKR activation via distinct mechanisms to avert fatal
685 autoinflammation. *Mol Cell* **83**: 3869-3884.e3867.
- 686 Huang HT, Seo HS, Zhang T, Wang Y, Jiang B, Li Q, Buckley DL, Nabet B, Roberts JM, Paulk J
687 et al. 2017. MELK is not necessary for the proliferation of basal-like breast cancer cells.
688 *Elife* **6**.
- 689 Huang W, Zhu Q, Shi Z, Tu Y, Li Q, Zheng W, Yuan Z, Li L, Zu X, Hao Y et al. 2024. Dual
690 inhibitors of DNMT and HDAC induce viral mimicry to induce antitumour immunity in
691 breast cancer. *Cell Death Discov* **10**: 143.
- 692 Ishizuka JJ, Manguso RT, Cheruiyot CK, Bi K, Panda A, Iracheta-Vellve A, Miller BC, Du PP,
693 Yates KB, Dubrot J et al. 2019. Loss of ADAR1 in tumours overcomes resistance to
694 immune checkpoint blockade. *Nature* **565**: 43-48.

- 695 Jeffrey IW, Kadereit S, Meurs EF, Metzger T, Bachmann M, Schwemmler M, Hovanessian AG,
696 Clemens MJ. 1995. Nuclear localization of the interferon-inducible protein kinase PKR in
697 human cells and transfected mouse cells. *Exp Cell Res* **218**: 17-27.
- 698 Jiang X, Muthusamy V, Fedorova O, Kong Y, Kim DJ, Bosenberg M, Pyle AM, Iwasaki A. 2019.
699 Intratumoral delivery of RIG-I agonist SLR14 induces robust antitumor responses. *J Exp*
700 *Med* **216**: 2854-2868.
- 701 Kim Y, Lee JH, Park JE, Cho J, Yi H, Kim VN. 2014. PKR is activated by cellular dsRNAs during
702 mitosis and acts as a mitotic regulator. *Genes Dev* **28**: 1310-1322.
- 703 Kumar A, Haque J, Lacoste J, Hiscott J, Williams BR. 1994. Double-stranded RNA-dependent
704 protein kinase activates transcription factor NF-kappa B by phosphorylating I kappa B.
705 *Proc Natl Acad Sci U S A* **91**: 6288-6292.
- 706 Kung CP, Cottrell KA, Ryu S, Bramel ER, Kladney RD, Bao EA, Freeman EC, Sabloak T, Maggi
707 L, Weber JD. 2021. Evaluating the therapeutic potential of ADAR1 inhibition for triple-
708 negative breast cancer. *Oncogene* **40**: 189-202.
- 709 Li S, Peters GA, Ding K, Zhang X, Qin J, Sen GC. 2006. Molecular basis for PKR activation by
710 PACT or dsRNA. *Proc Natl Acad Sci U S A* **103**: 10005-10010.
- 711 Liberzon A, Birger C, Thorvaldsdóttir H, Ghandi M, Mesirov JP, Tamayo P. 2015. The Molecular
712 Signatures Database (MSigDB) hallmark gene set collection. *Cell Syst* **1**: 417-425.
- 713 Liddicoat BJ, Piskol R, Chalk AM, Ramaswami G, Higuchi M, Hartner JC, Li JB, Seeburg PH,
714 Walkley CR. 2015. RNA editing by ADAR1 prevents MDA5 sensing of endogenous
715 dsRNA as nonself. *Science* **349**: 1115-1120.
- 716 Liu H, Golji J, Brodeur LK, Chung FS, Chen JT, deBeaumont RS, Bullock CP, Jones MD, Kerr
717 G, Li L et al. 2019. Tumor-derived IFN triggers chronic pathway agonism and sensitivity
718 to ADAR loss. *Nat Med* **25**: 95-102.
- 719 Lu T, Ma P, Fang H, Chen A, Xu J, Kuang X, Wang M, Su L, Wang S, Zhang Y et al. 2025.
720 Prkra dimer senses double-stranded RNAs to dictate global translation efficiency. *Mol*
721 *Cell* **85**: 2032-2047.e2039.
- 722 Manjunath L, Santiago G, Ortega P, Sanchez A, Oh S, Garcia A, Li J, Duong D, Bournique E,
723 Bouin A et al. 2025. Cooperative role of PACT and ADAR1 in preventing aberrant PKR
724 activation by self-derived double-stranded RNA. *Nat Commun* **16**: 3246.
- 725 Matsumoto M, Oshiumi H, Seya T. 2011. Antiviral responses induced by the TLR3 pathway.
726 *Rev Med Virol* **21**: 67-77.
- 727 McFarland JM, Ho ZV, Kugener G, Dempster JM, Montgomery PG, Bryan JG, Krill-Burger JM,
728 Green TM, Vazquez F, Boehm JS et al. 2018. Improved estimation of cancer
729 dependencies from large-scale RNAi screens using model-based normalization and data
730 integration. *Nat Commun* **9**: 4610.
- 731 Mendoza HG, Beal PA. 2024. Structural and functional effects of inosine modification in mRNA.
732 *RNA* **30**: 512-520.
- 733 Meyer C, Garzia A, Mazzola M, Gerstberger S, Molina H, Tuschl T. 2018. The TIA1 RNA-
734 Binding Protein Family Regulates EIF2AK2-Mediated Stress Response and Cell Cycle
735 Progression. *Mol Cell* **69**: 622-635.e626.
- 736 Morad G, Helmink BA, Sharma P, Wargo JA. 2021. Hallmarks of response, resistance, and
737 toxicity to immune checkpoint blockade. *Cell* **184**: 5309-5337.
- 738 Novoa I, Zeng H, Harding HP, Ron D. 2001. Feedback inhibition of the unfolded protein
739 response by GADD34-mediated dephosphorylation of eIF2alpha. *J Cell Biol* **153**: 1011-
740 1022.
- 741 Park H, Davies MV, Langland JO, Chang HW, Nam YS, Tartaglia J, Paoletti E, Jacobs BL,
742 Kaufman RJ, Venkatesan S. 1994. TAR RNA-binding protein is an inhibitor of the
743 interferon-induced protein kinase PKR. *Proc Natl Acad Sci U S A* **91**: 4713-4717.

- 744 Patel CV, Handy I, Goldsmith T, Patel RC. 2000. PACT, a stress-modulated cellular activator of
745 interferon-induced double-stranded RNA-activated protein kinase, PKR. *J Biol Chem*
746 **275**: 37993-37998.
- 747 Patel RC, Sen GC. 1998. PACT, a protein activator of the interferon-induced protein kinase,
748 PKR. *EMBO J* **17**: 4379-4390.
- 749 Pestal K, Funk CC, Snyder JM, Price ND, Treuting PM, Stetson DB. 2015. Isoforms of RNA-
750 Editing Enzyme ADAR1 Independently Control Nucleic Acid Sensor MDA5-Driven
751 Autoimmunity and Multi-organ Development. *Immunity* **43**: 933-944.
- 752 Peters GA, Dickerman B, Sen GC. 2009. Biochemical analysis of PKR activation by PACT.
753 *Biochemistry* **48**: 7441-7447.
- 754 Peters GA, Hartmann R, Qin J, Sen GC. 2001. Modular structure of PACT: distinct domains for
755 binding and activating PKR. *Mol Cell Biol* **21**: 1908-1920.
- 756 Rehwinkel J, Gack MU. 2020. RIG-I-like receptors: their regulation and roles in RNA sensing.
757 *Nat Rev Immunol* **20**: 537-551.
- 758 Singh M, Castillo D, Patel CV, Patel RC. 2011. Stress-induced phosphorylation of PACT
759 reduces its interaction with TRBP and leads to PKR activation. *Biochemistry* **50**: 4550-
760 4560.
- 761 Sinigaglia K, Cherian A, Du Q, Lacovich V, Vukić D, Melicherová J, Linhartova P, Zerad L,
762 Stejskal S, Malik R et al. 2024. An ADAR1 dsRBD3-PKR kinase domain interaction on
763 dsRNA inhibits PKR activation. *Cell Rep* **43**: 114618.
- 764 Stewart SA, Dykxhoorn DM, Palliser D, Mizuno H, Yu EY, An DS, Sabatini DM, Chen IS, Hahn
765 WC, Sharp PA et al. 2003. Lentivirus-delivered stable gene silencing by RNAi in primary
766 cells. *RNA* **9**: 493-501.
- 767 Stringer BW, Day BW, D'Souza RCJ, Jamieson PR, Ensbey KS, Bruce ZC, Lim YC, Goasdoué
768 K, Offenhäuser C, Akgül S et al. 2019. A reference collection of patient-derived cell line
769 and xenograft models of proneural, classical and mesenchymal glioblastoma. *Sci Rep* **9**:
770 4902.
- 771 Takahashi T, Miyakawa T, Zenno S, Nishi K, Tanokura M, Ui-Tei K. 2013. Distinguishable in
772 vitro binding mode of monomeric TRBP and dimeric PACT with siRNA. *PLoS One* **8**:
773 e63434.
- 774 Valente L, Nishikura K. 2007. RNA binding-independent dimerization of adenosine deaminases
775 acting on RNA and dominant negative effects of nonfunctional subunits on dimer
776 functions. *J Biol Chem* **282**: 16054-16061.
- 777 Waks AG, Winer EP. 2019. Breast Cancer Treatment: A Review. *JAMA* **321**: 288-300.
- 778 Wong YL, LeBon L, Basso AM, Kohlhaas KL, Nikkel AL, Robb HM, Donnelly-Roberts DL,
779 Prakash J, Swensen AM, Rubinstein ND et al. 2019. eIF2B activator prevents
780 neurological defects caused by a chronic integrated stress response. *Elife* **8**.
- 781 Young AA, Bohlin HE, Pierce JR, Cottrell KA. 2024. Suppression of double-stranded RNA
782 sensing in cancer: molecular mechanisms and therapeutic potential. *Biochem Soc*
783 *Trans*.
- 784 Zamanian-Daryoush M, Mogensen TH, DiDonato JA, Williams BR. 2000. NF-kappaB activation
785 by double-stranded-RNA-activated protein kinase (PKR) is mediated through NF-
786 kappaB-inducing kinase and IkappaB kinase. *Mol Cell Biol* **20**: 1278-1290.
- 787 Zou T, Zhou M, Gupta A, Zhuang P, Fishbein AR, Wei HY, Capcha-Rodriguez D, Zhang Z,
788 Cherniack AD, Meyerson M. 2024. XRN1 deletion induces PKR-dependent cell lethality
789 in interferon-activated cancer cells. *Cell Rep* **43**: 113600.

791

792

793 **Figure 1: PACT is a co-dependency of ADAR1 and is essential in many TNBC cell lines**
794 **a** and **c** Volcano plots of Pearson correlation coefficients and FDR corrected p-values for
795 pairwise comparisons between ADAR1 CHRONOS score (**a**) or PACT CHRONOS score (**c**)
796 and CHRONOS scores for all genes in DepMap across all cell lines. **b** Correlation between
797 PACT and ADAR1 CHRONOS scores for all DepMap cell lines, Pearson correlation coefficient
798 and p-value shown. **d** Top, density plot of CHRONOS scores for PACT or all other genes.
799 Bottom, boxplots for PACT CHRONOS score by lineage. **e** Correlation between PACT and
800 ADAR1 CHRONOS scores for breast cancer cell lines, Pearson correlation coefficient and p-
801 value shown. **f** Boxplot of PACT CHRONOS Scores of breast cancer cell lines separated by
802 subtype. **g** Left, CHRONOS score difference between TNBC and non-TNBC cell lines. Right,
803 CHRONOS Score box plots for TNBC and non-TNBC cell lines. The top five genes based on
804 the difference of CHRONOS scores between TNBC and non-TNBC are shown. All data shown
805 from DepMap.

806

807 **Figure 2: PACT is highly expressed in TNBC**

808 Expression of PACT at the RNA (**a**) or protein level (**b**) in breast cancer cell lines separated by
809 subtype. **c** Representative immunoblot for PACT and ADAR1 expression in a panel of breast
810 cancer cell lines. Cell lines in blue are PACT-independent and purple are PACT-dependent.
811 Total protein was imaged using a Stain-Free Gel and serves as a loading control. **d - e**
812 Expression of PACT at the RNA level in normal and breast tumor samples separated by
813 subtypes. **e - f** Overall survival of breast cancer patients separated by high or low PACT
814 expression for all tumor types (**e**) or TNBC only (**f**). For panels **a,b,d** and **e**, data from DepMap;
815 **f, g** from TCGA.

816

817 **Figure 3: PACT overexpression does not cause PKR activation in TNBC**

818 **a** Representative immunoblots for proteins of interest in control (empty vector, EV) or PACT
819 (PACT, PACT S287A, PACT S287D) overexpressing cell lines. The blots for each cell line were
820 performed independently and should not be compared between cell lines. Total protein was
821 imaged using a Stain-Free Gel and was used as the loading control for normalization. **b**
822 Quantification of the blot in **a**. Bars represent the average of at least three biological replicates,
823 error bars are +/- SD. **c** and **d** Scatter plots comparing the protein abundance of PACT (**c**) or
824 ATF3 (**d**) to ATF4 protein abundance across cancer cell lines, the Pearson correlation
825 coefficient and p-value are shown. Data for **c** and **d** from DepMap.

826

827 **Figure 4: In PACT-dependent TNBC cells, PACT is required for viability, tumorigenesis,**
828 **and suppression of PKR activation**

829 **a** Correlation between PACT and ADAR1 CHRONOS scores of breast cancer cell lines,
830 Pearson correlation coefficient and p-value shown, data from DepMap. The labeled cell lines
831 are used in PACT depletion experiments. **b** Representative immunoblot for PACT-independent
832 and PACT-dependent cell lines with (sgPACT-1, sgPACT-2) or without (sgNTA, sgC1) depletion
833 of PACT. The blots for each cell line were performed independently and should not be
834 compared between cell lines. Total protein was imaged using a Stain-Free Gel and was used as
835 the loading control for normalization. **c** Cell viability as assessed by CellTiter-Glo 2.0 in PACT
836 depleted and control cell lines. **d** Representative crystal violet staining of PACT depleted and
837 control cells. **e** Effect of PACT depletion on tumorigenesis of HCC1806 cells. Left panel is tumor
838 volume over time, right panel is the final tumor volume at end-point. **f** Quantification of the
839 immunoblot in **b**. Bars represent the average of at least four biological replicates, error bars are
840 +/- SD. * p < 0.05, ** p < 0.01, *** p < 0.001. P-values determined by one-way ANOVA with post-
841 hoc Tukey (**c** and **f**), or t-test (**e**).

842

843 **Figure 5: PACT depletion does not cause activation of type I IFN or RNaseL**

844 **a** and **b** Volcano plot for fold-change of RNA expression in PACT depleted (sgPACT-2) or
845 control (sgC1 or sgNTA) HCC1806 (**a**) or MDA-MB-468 (**b**). **c** Heatmap for RNA expression of
846 type I ISGs (genes belonging to the gene set: Hallmark interferon alpha response). Top panel,
847 box and overlaid 'quasirandom' plots for all ISGs in the heatmap below. The heatmap is
848 clustered by gene (rows), the dendrogram has been omitted for brevity. **d** qRT-PCR for RNA
849 expression for ISGs in PACT depleted and control cells. Bars represent the average of at least
850 four biological replicates, error bars are +/- SD. **e** Representative psuedo-gel images of rRNA
851 integrity for PACT depleted and control cells.

852

853 **Figure 6: PKR is required for activation of NF- κ B and ISR upon PACT depletion**

854 **a** Dot blot summarizing the gene sets that are significantly up or downregulated in PACT
855 depleted cells. FDR is the FDR corrected p-value for each gene set. **b** and **c**, qRT-PCR for RNA
856 expression for ATF4 targets (**b**) or NF- κ B targets (**c**) in PACT depleted and control cells. **d**
857 Representative immunoblot of PACT depleted and control HCC1806 EV (empty vector) cells.
858 Total protein was imaged using a Stain-Free Gel and was used as the loading control for
859 normalization. **e** Representative immunoblot for control (sgC1/sgNTA), PACT depleted
860 (sgC1/sgPACT-2), PKR depleted (sgC1/sgPKR) or combined depleted cell lines
861 (sgPKR/sgPACT-2). **f** Cell viability as assessed by CellTiter-Glo 2.0 for the same conditions as
862 **e**. **g** qRT-PCR for RNA expression for ATF4 targets or NF- κ B targets for the same conditions as
863 **e**. Bars represent the average of at least four biological replicates, error bars are +/- SD. * p
864 <0.05, ** p <0.01, *** p < 0.001. P-values determined by Dunnett's test.

865

866 **Figure 7: PACT dsRNA binding and dimerization is required for suppression of PKR** 867 **activation**

868 **a** Alignment of dsRBD 1 and 2 of PACT and dsRBDs 1-3 of ADAR1. The amino acid
869 substitutions made for disrupting PACT dsRNA binding are shown below. **b** Representative

870 immunoblot for control (sgNTA) and PACT depleted (sgPACT-2), with (PACT, PACT-EAA,
871 PACT-AA) or without (EV, empty vector) overexpression of WT or dsRNA binding mutant PACT.
872 **c** Quantification of the immunoblots in **b**. **d** Cell viability as assessed by CellTiter-Glo 2.0 for the
873 same conditions as **b**. **e** Domain structure of WT PACT and PACT truncation and fusion
874 constructs. **f** Representative immunoblot for control (sgNTA) and PACT depleted (sgPACT-2),
875 with (PACT, PACT^{Δd3} or PACT^{Δd3}-GST) or without (EV, empty vector) overexpression of WT or
876 truncated PACT. **g** Quantification of the immunoblots in **f**. **h** Cell viability as assessed by
877 CellTiter-Glo 2.0 for the same conditions as **f**. Bars represent the average of at least three
878 replicates, error bars are +/- SD. * p < 0.05, ** p < 0.01, *** p < 0.001. P-values determined by
879 Dunnett's test.

880

881 **Figure 8: PACT and ADAR1 function redundantly to suppress PKR activation in**

882 **PACT/ADAR1-independent cell lines**

883 **a** Representative immunoblot for control (sgC1, sgNTA) and PACT depleted (sgPACT-1,
884 sgPACT-2), with (shADAR1) or without (shSCR) knockdown of ADAR1. **b** Cell viability as
885 assessed by CellTiter-Glo 2.0 for the same conditions as **a**. **c** Quantification of the immunoblots
886 in **a**. **d-f** qRT-PCR for RNA expression of ATF4 targets (**d**), NF-κB targets (**e**) or ISGs (**f**) for the
887 same conditions as **a**, MDA-MB-453. **g** Representative psuedo-gel images of rRNA integrity for
888 the same conditions as **a**, MDA-MB-453. **h** Representative immunoblot for control (sgNTA) and
889 PACT depleted (sgPACT-2), with (p110, p150) or without (EV, empty vector) overexpression of
890 ADAR1 isoforms. **i** Quantification of the immunoblots in **h**. **j** Cell viability as assessed by
891 CellTiter-Glo 2.0 for the same conditions as **h**. Bars represent the average of at least three
892 replicates, error bars are +/- SD. * p < 0.05, ** p < 0.01, *** p < 0.001. P-values determined by
893 one-way ANOVA with post-hoc Tukey (**b** and **c**), or Dunnett's test (**i** and **j**).

894

895 **Figure 9: PKR expression is elevated in breast cancer and correlates with PACT-**
896 **dependency**

897 **a – b** Scatter plots comparing ISG expression (Core ISG Score, described previously (Kung et
898 al. 2021)) and either ADAR1-dependency score (ADAR CHRONOS Score, **a**) or PACT-
899 dependency score (PACT CHRONOS Score, **b**). **c** Scatter plot comparing PKR protein
900 abundance and PACT-dependency score. For all scatter plots, the Pearson correlation
901 coefficient and p-values are shown. **d** Summary of Pearson correlation coefficients and p-values
902 between PKR protein abundance and PACT-dependency score for cancer cell line lineages.
903 Lineages with PKR abundance and PACT-dependency scores for fewer than four cell lines were
904 omitted. **e** Representative immunoblot for PKR and P-PKR in TNBC cell lines. Total protein is a
905 Stain-Free gel image used as a loading control. **f** PKR protein abundance in breast cancer cell
906 lines separated by subtype. **g** and **h** PKR RNA expression in normal human breast and breast
907 tumors, data from TCGA. **i** Model for cellular sensitivity to depletion of ADAR1 and/or PACT. For
908 panels **a-d** and **f**, data from DepMap; **g-h** from TCGA.

909

910

911

912

FIGURE 1

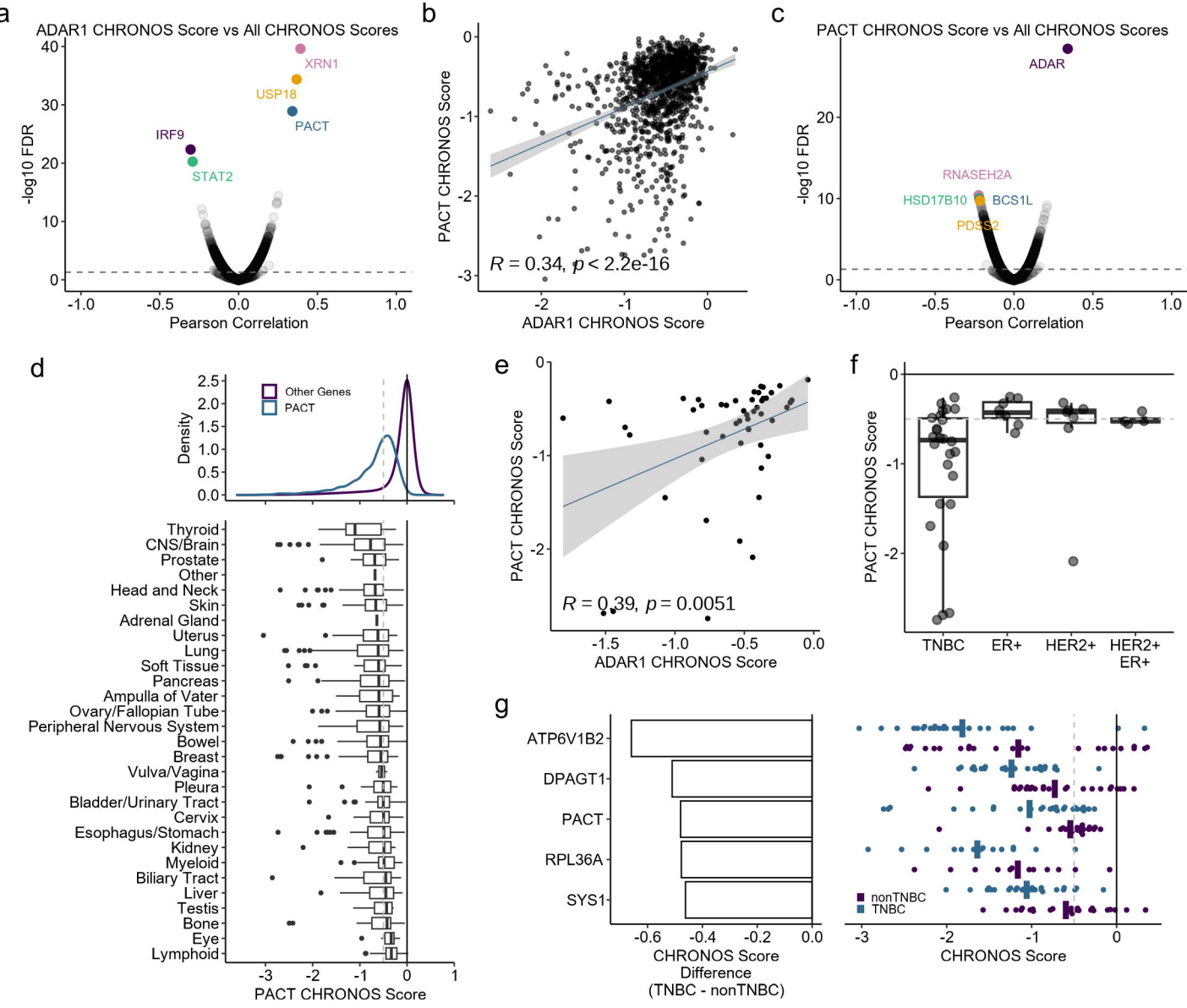


FIGURE 2

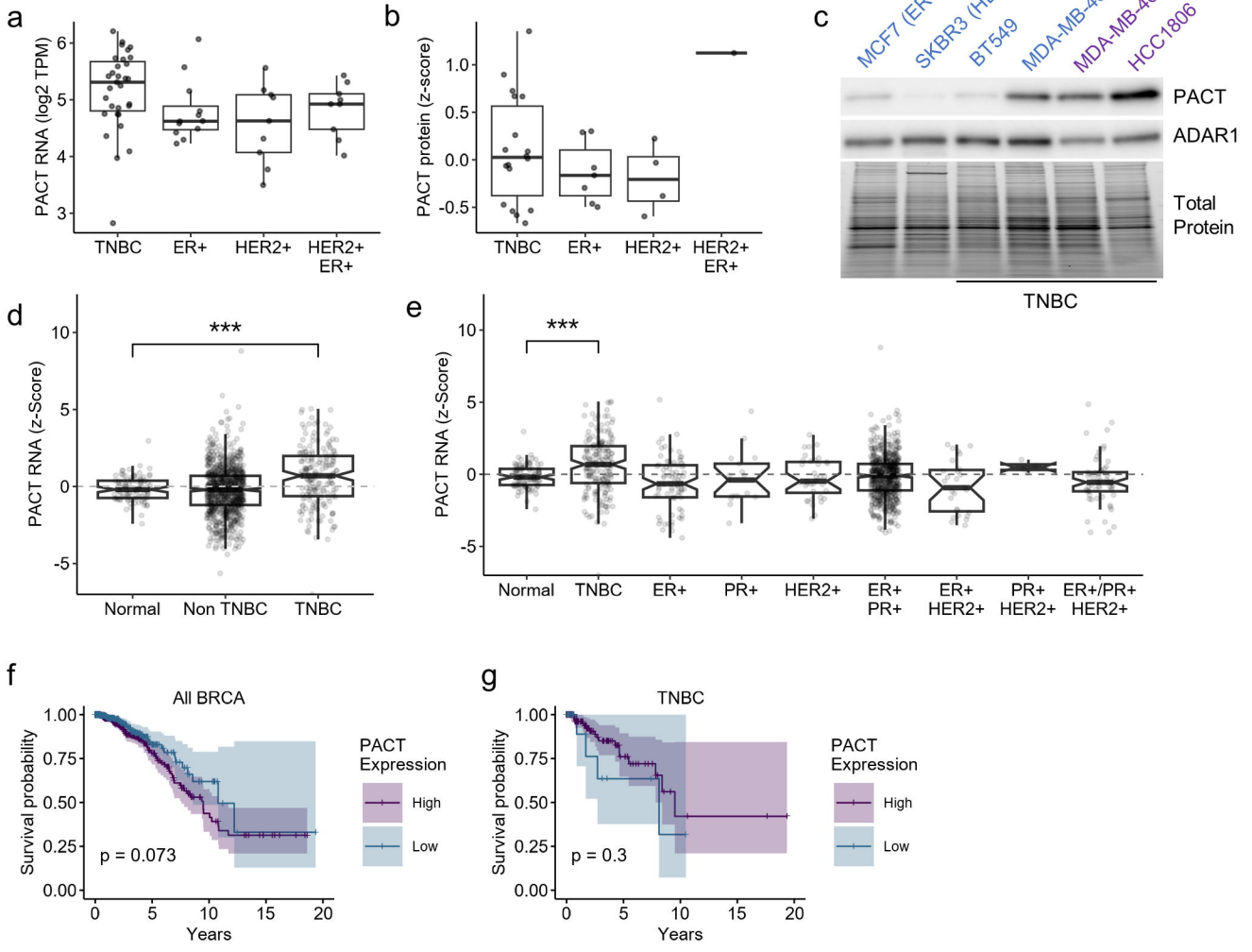


FIGURE 3

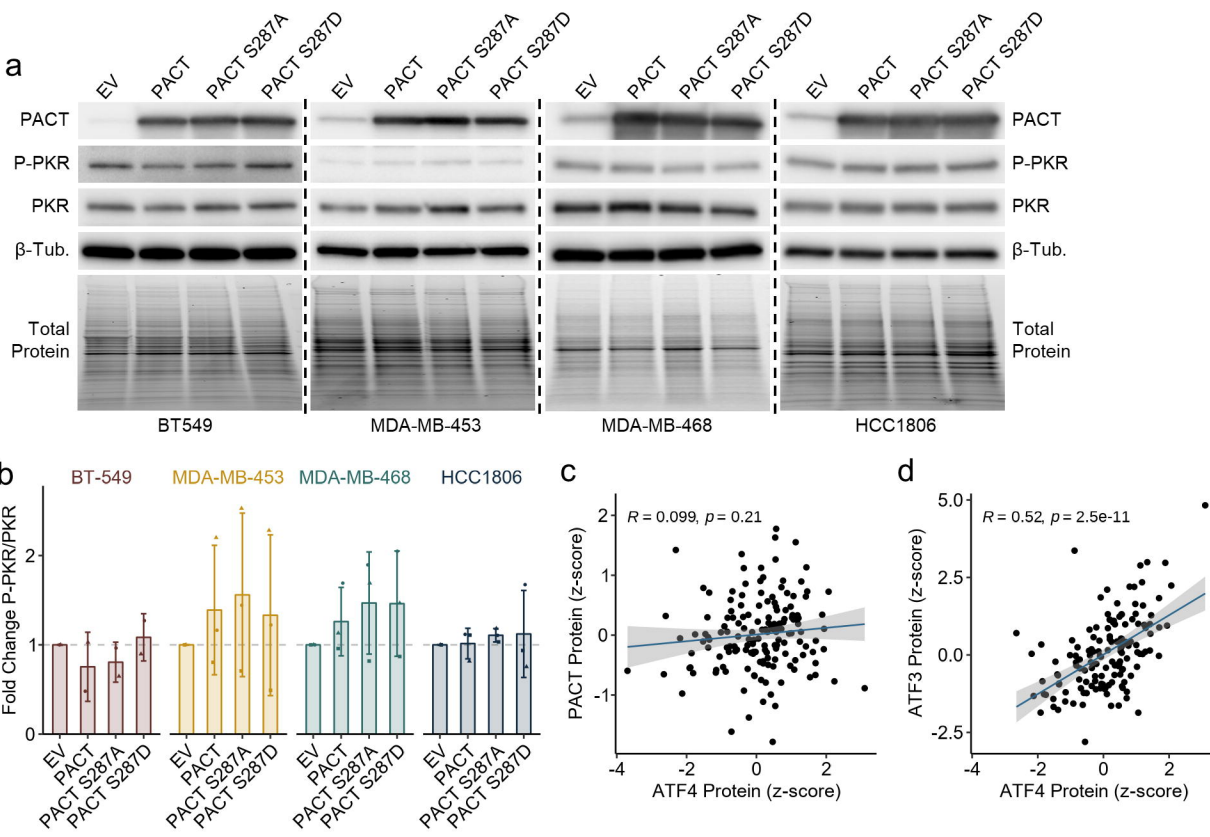


FIGURE 4

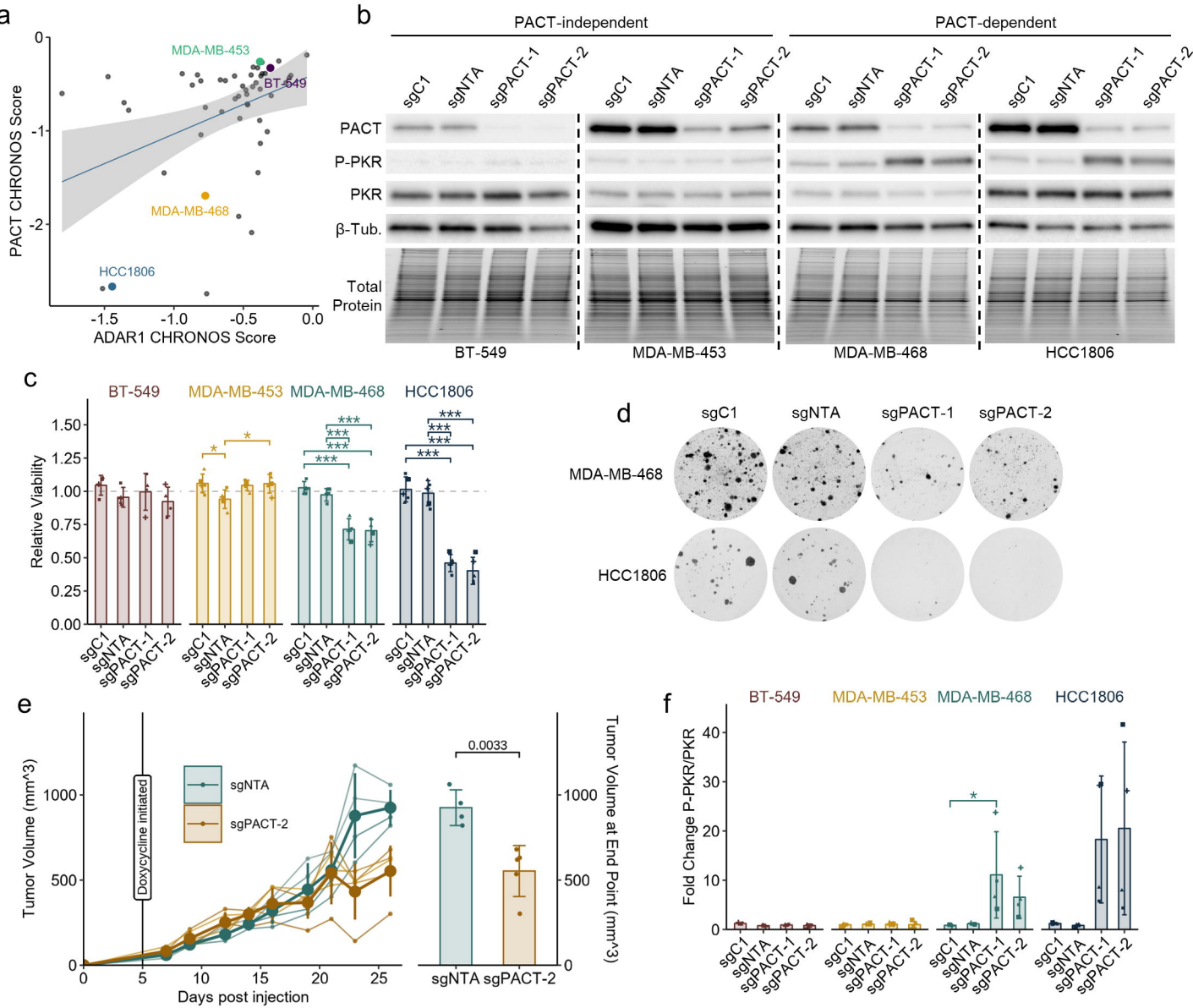


FIGURE 5

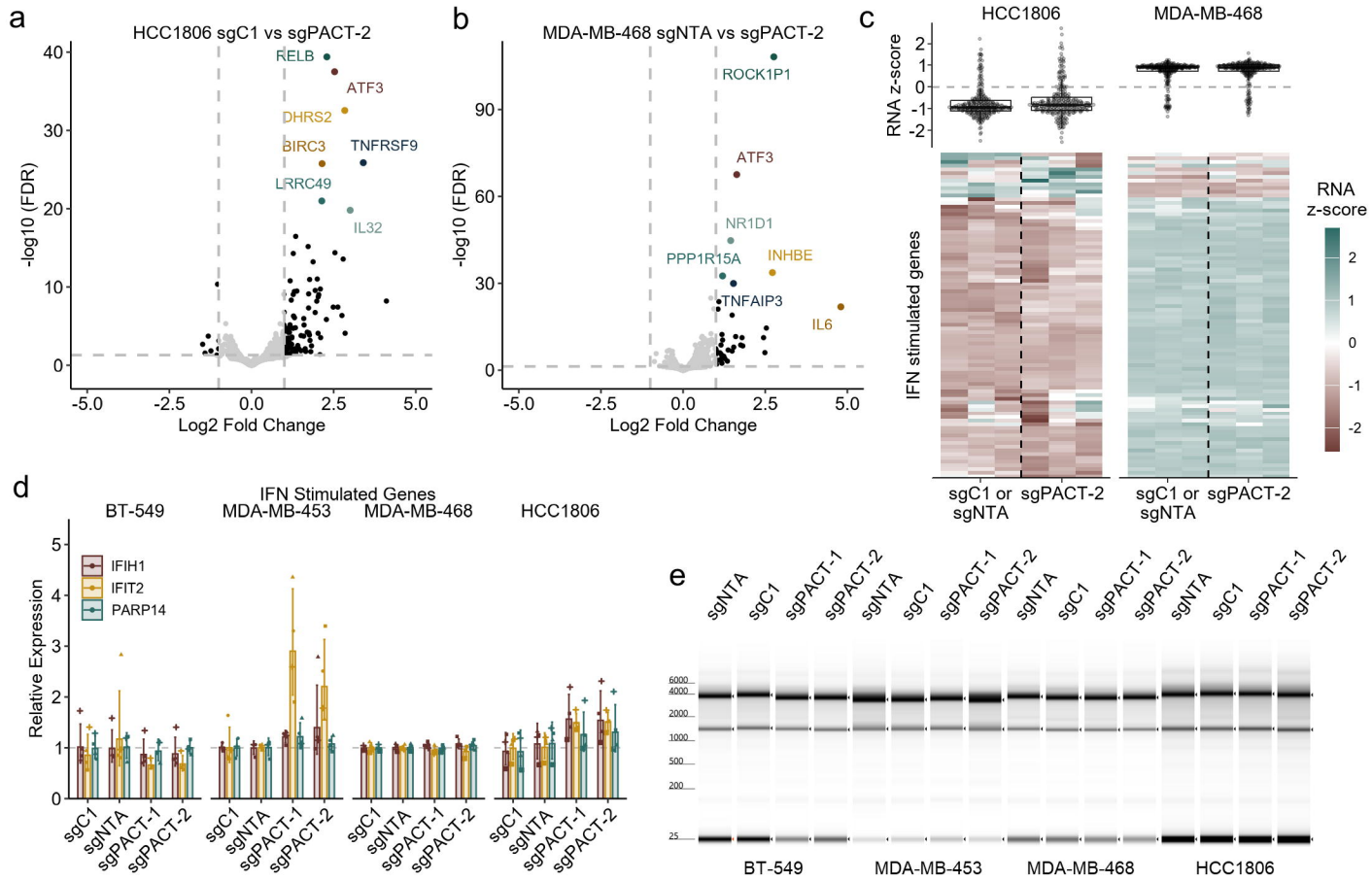


FIGURE 6

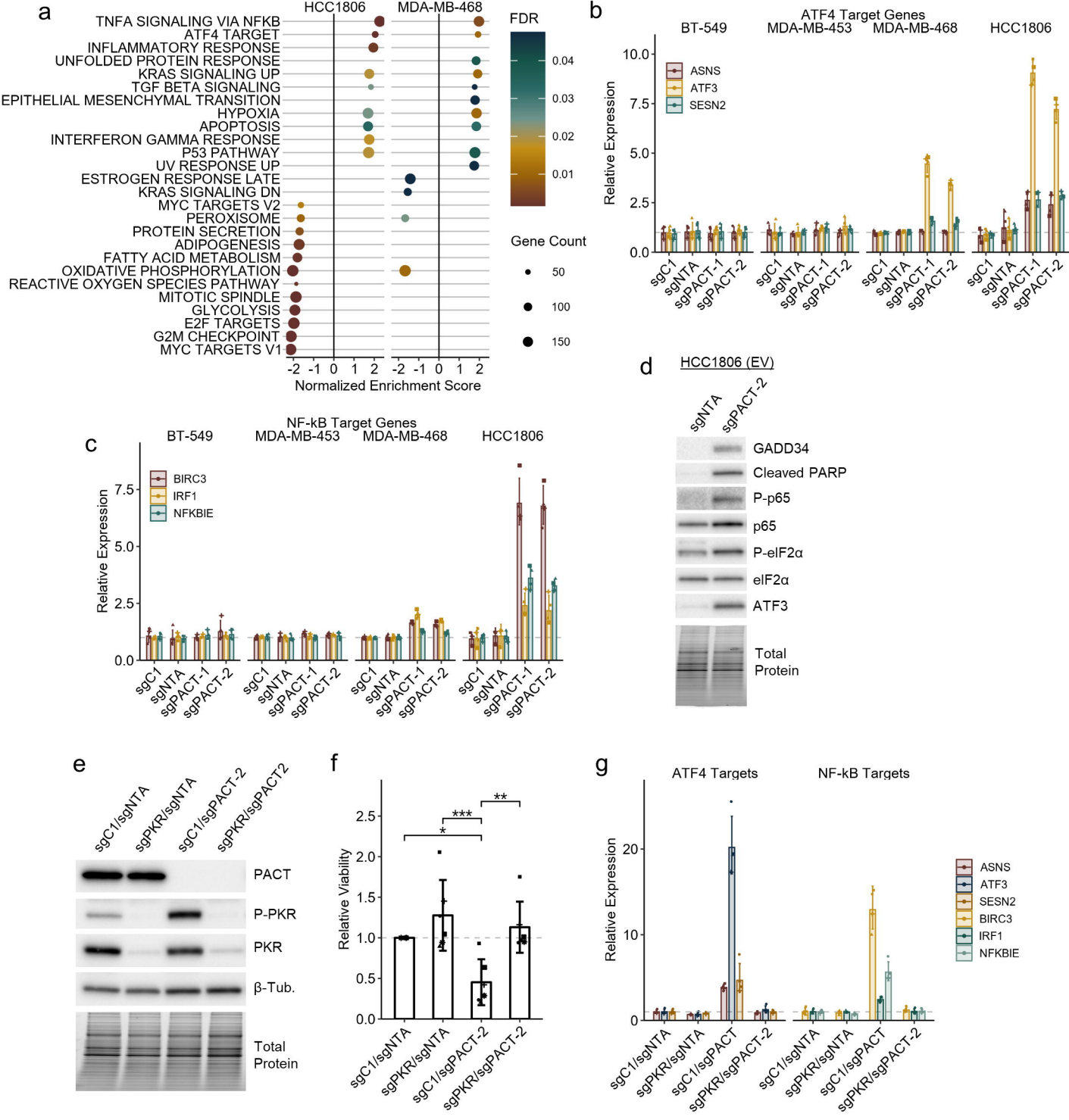
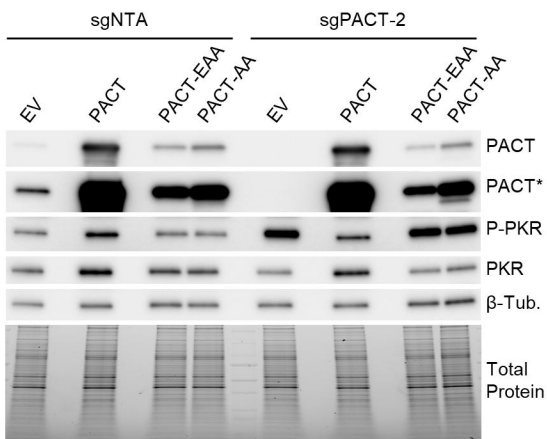


FIGURE 7

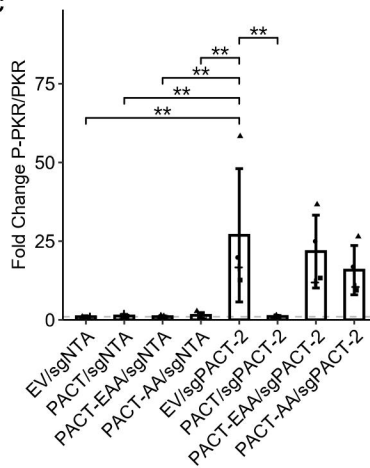
a

PACT-dsRBD2 NPIGSLQELAIHHGWRLPEYTLSEQGGPAHKREYTTICRLES-FMETGKGASKRQAKRNAAEKFLAKFSN
 PACT-dsRBD1 TPIQVLHEYGMKTKN-IPVYECERSDVQIHVPTFTFRVTVGDI TCT-GEGTSKRLAKHRAAEAAINILKA
 ADAR1-dsRBD2 SPVTTLLECMHKLGN-SCEFRLLSKEGPAHEPKFYQCVAVGAQTFPSPVSAPS KIKVAKQMAAEEAMKALHG
 ADAR1-dsRBD1 NPISGLLEYAQFASQ-TCEFNMIEQSGPPHEPRFKFQVVINGREFPPAEAGSKIKVAKQDAAMKAMTILLE
 ADAR1-dsRBD3 NPVGGLELEYARSHGF-AAEFKLVQSGPPHEPKFVYQAKVGGRWFPVAVCAHSKRQGRQEAADAALRVLIG
 .*: * * : . * : : . * * . : * * : :
 PACT-EAA -----EA--A-
 PACT-AA -----AA--

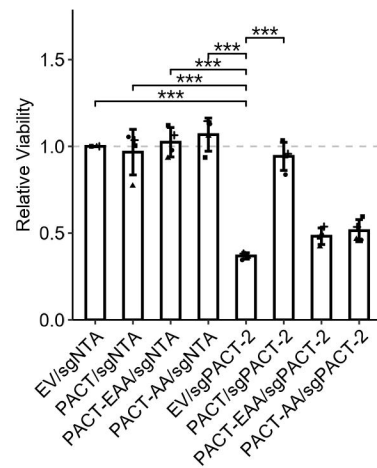
b



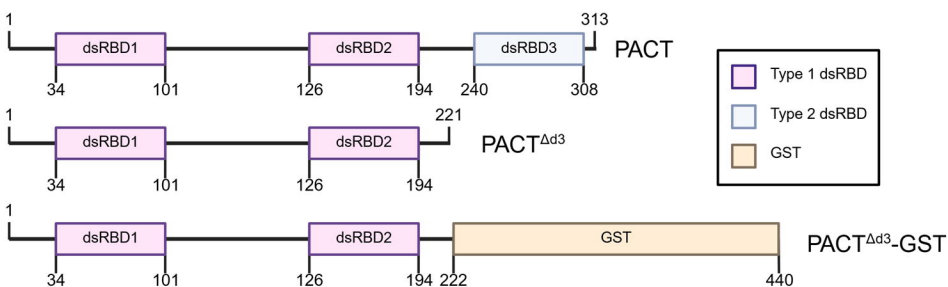
c



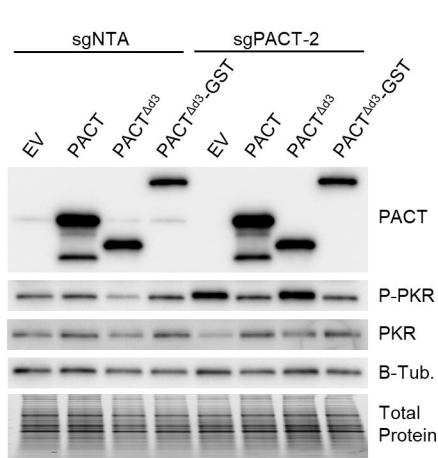
d



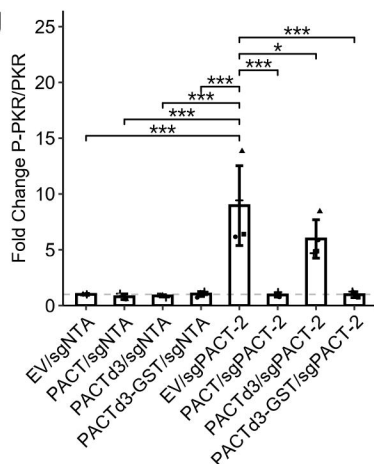
e



f



g



h

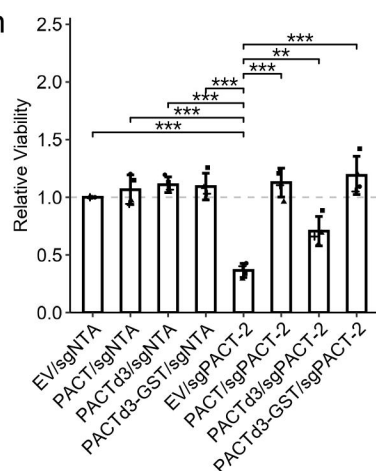
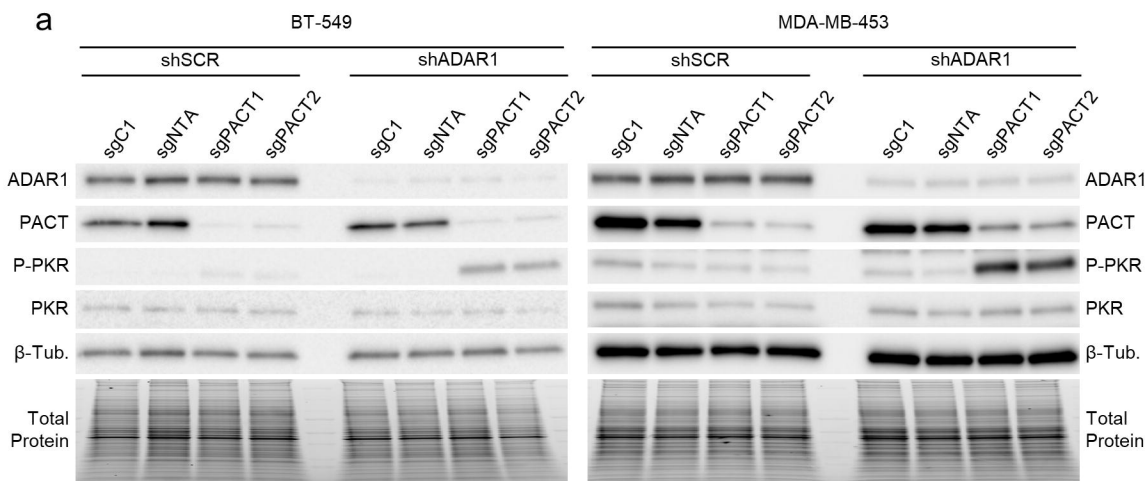
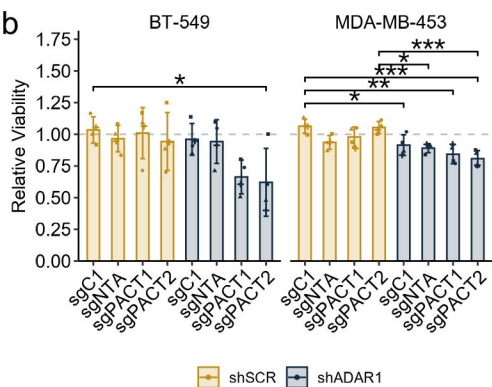


FIGURE 8

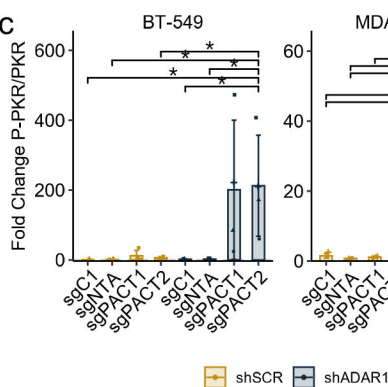
a



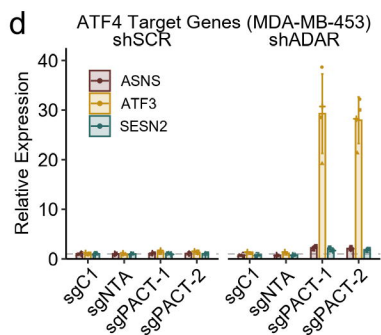
b



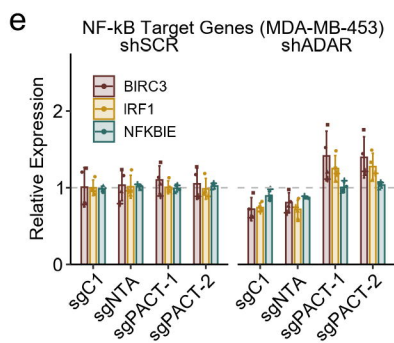
c



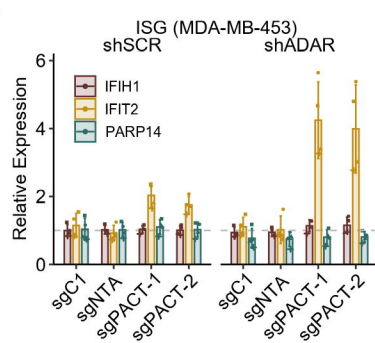
d



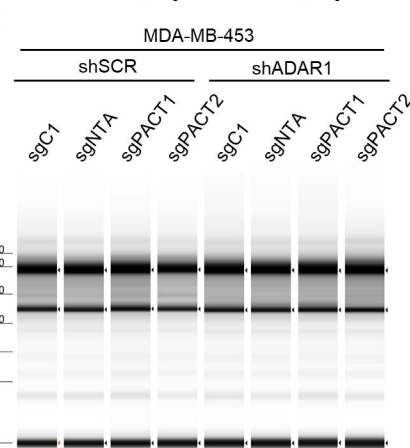
e



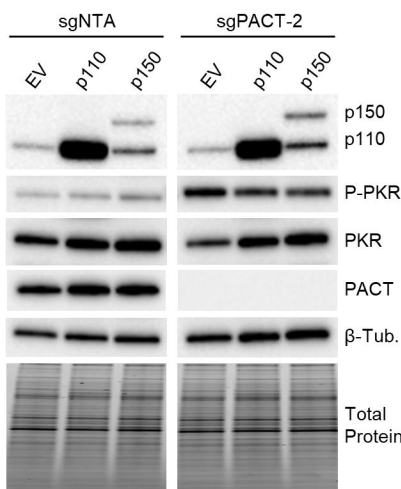
f



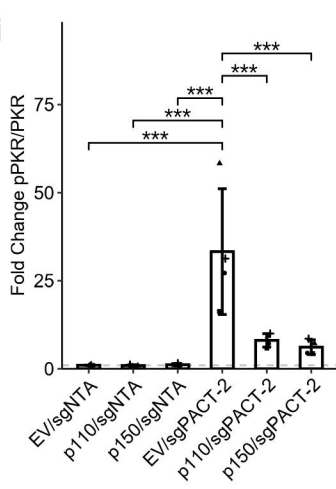
g



h



i



j

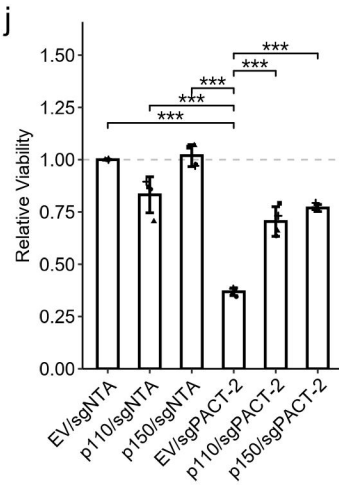


FIGURE 9

